To the Graduate Council:

I am submitting herewith a thesis written by Michael John Christiansen entitled "Analysis of Magnetohydrodynamic Acceleration for use in Hypersonic Direct-Connect Propulsion Testing." I have examined the final copy of this thesis for form and content and recommended that it will be accepted in partial fulfillment of the requirements for the degree of Master of Science, with a major in Mechanical Engineering.

Harold J. Schmidt, Major Professor

We have read this thesis
and recommend its acceptance:

Roger Crawford

James N. Chapman

Accepted for the Council:

Associate Vice Chancellor
and Dean of The Graduate School

STATEMENT OF PERMISSION TO USE

In presenting this thesis in partial fulfillment of the requirements for a Master's degree at the University of Tennessee, Knoxville, I agree that the Library shall make it available to borrowers under the rules of the Library. Brief quotations from this thesis are allowable without special permission, provided that accurate acknowledgement of the source is made.

Permission for extensive quotation from or reproduction of this thesis may be granted by my major professor, or in his absence, by the Head of Interlibrary Services when, in the opinion of either, the proposed use of the material is for scholarly purposes. Any copying or use of the material in this thesis for financial gain shall not be allowed without my written permission.

Signature Michael Christiansen

Date May 22, 1995

ANALYSIS OF MAGNETOHYDRODYNAMIC ACCELERATION FOR USE IN HYPERSONIC DIRECT-CONNECT PROPULSION TESTING

A Thesis

Presented for the

Master of Science

Degree

The University of Tennessee, Knoxville

Michael John Christiansen

August 1995

ACKNOWLEDGMENTS

I would like to thank my committee members for the time and effort they spent helping me prepare this thesis. Dr. Harold Schmidt, my major professor, spent countless hours reviewing and advising on this thesis. Dr. James Chapman accepted me as a Graduate Research Assistant and taught me all that I know about MHD. Dr. Roger Crawford helped me to gain insight on the physical meaning of my work. For all their guidance and suggestions, I give them great thanks.

I would also like to thank Bob Rhodes for the use of his LAPP code, and the training and technical assistance he gave along with it. The entire computer staff at UTSI has been a great help to me along the way, especially Rich Tito, who rebooted the network at night when it crashed. There are countless others at UTSI who have lent a hand in this thesis, and I thank them all for their help. Finally I would like to thank my family for the support they have given me all of my life.

ABSTRACT

A previously completed UTSI study of the use of an MHD accelerator with seeded air from a state-of-the-art arc heater, was generally accepted as showing that the system studied had some promise of meeting the most critical hypersonic testing requirements. However, some concerns existed about certain aspects of the results. This thesis discusses some of these problems and presents analysis of potential solutions. Specifically the goals addressed were to alleviate the problems of: reducing the amount of seed in the flow, reducing test chamber flow temperature, and reducing the oxygen dissociation.

Modeling techniques are used to study three design variables of the MHD accelerator. The accelerator channel inlet Mach number, the accelerator channel divergence angle, and the magnetic field strength are all studied. These variables are all optimized to meet the goals of seed, temperature, and dissociated oxygen reduction.

The results of this thesis are encouraging, showing that hypersonic testing environments can be produced. Analytical solutions that satisfy all three goals of the thesis are presented and discussed in detail. This thesis extends the results previously reported by UTSI and further demonstrates the feasibility of MHD acceleration as a viable means to provide hypersonic flight simulation.

TABLE OF CONTENTS

Page

1.0 INTRODUCTION 1

1.1 The History of MHD Acceleration for Hypersonic Simulation ... 1

1.2 A Brief Summary of the UTSI Investigation 5

1.3 Investigation Goals 6

1.4 Investigation Limits 8

1.5 Method of Development 8

2.0 SIMULATION REQUIREMENTS 10

2.1 Hypersonic Flight Envelope 10

2.2 True-Air Conditions 12

2.3 Direct-Connect Propulsion Testing 14

3.0 MODEL OF DIRECT-CONNECT MHD ACCELERATOR HYPERSONIC WIND TUNNEL 16

3.1 Upstream Simulation 17

3.2 MHD Accelerator Simulation 18

3.3 Downstream Simulation 21

4.0 MHD ACCELERATOR TRADE-OFF STUDIES 23

4.1 Baseline Channel Design 23

4.2 Accelerator Entrance Mach Number 26

4.3 Accelerator Channel Divergence Angle 33

Page

4.4 Magnetic Field Strength 39

4.5 Optimum Accelerator Configuration 45

4.6 Results for Other Mach Numbers 55

5.0 CONCLUSIONS AND RECOMMENDATIONS 60

5.1 Channel Design Trade-Off Study Conclusions 60

5.2 Recommendations for Future Study 62

LIST OF REFERENCES 64

VITA 66

LIST OF TABLES

Table **Page**

4.1 Baseline Accelerator Performance 24

4.2 Accelerator Channel Inlet Mach Number Cases 27

4.3 Accelerator Performance (Inlet Mach = 3.01) 32

4.4 Channel Divergence Angle Input Cases 33

4.5 Accelerator Performance (Angle = 0.8°) 38

4.6 Accelerator Performance (12 Tesla Field) 44

4.7 Accelerator Performance (Mach = 3.38, 16 Tesla Field) 49

4.8 Accelerator Performance (Angle = 0.9°, 12 Tesla Field, 2.0% K) .. 52

4.9 Accelerator Performance (Angle = 0.9°, 16 Tesla Field, 0.5% K) .. 54

4.10 Accelerator Performance (Mach 25 Simulation) 57

4.11 Accelerator Performance (Mach 15 Simulation) 58

LIST OF FIGURES

Figure		Page
1.1	Simple MHD Generator	2
1.2	Simple MHD Accelerator	3
2.1	Hypersonic Flight Envelope	11
2.2	Conductivity of Air with 2.0 Percent Potassium	13
2.3	Conductivity of Air with 0.5 Percent Potassium	13
2.4	Combustor Test Conditions for q = 1000 psf	14
3.1	MHD Augmented Direct-Connect Simulation Facility	16
4.1	Baseline Accelerator Performance	25
4.2	Current Density versus Channel Inlet Mach Number	28
4.3	Exit Entropy versus Channel Inlet Mach Number	29
4.4	Downstream Nozzle Area Ratio versus Channel Inlet Mach Number	29
4.5	Temperature versus Channel Inlet Mach Number	31
4.6	Dissociated Oxygen versus Channel Inlet Mach Number	31
4.7	Accelerator Performance (Mach = 3.01)	32
4.8	Current Density versus Channel Divergence Angle	35
4.9	Exit Entropy versus Channel Divergence Angle	35
4.10	Downstream Nozzle Area Ratio versus Channel Divergence Angle	36
4.11	Temperature versus Channel Divergence Angle	36

Page

4.12 Dissociated Oxygen versus Channel Divergence Angle 37

4.13 Accelerator Performance (Angle = 0.8°) 38

4.14 Current Density versus Magnetic Field Strength 40

4.15 Exit Entropy versus Magnetic Field Strength 40

4.16 Downstream Nozzle Area Ratio versus Magnetic Field Strength ... 42

4.17 Temperature versus Magnetic Field Strength 42

4.18 Dissociated Oxygen versus Magnetic Field Strength 43

4.19 Accelerator Performance (12 Tesla Field) 44

4.20 Temperature versus Magnetic Field Strength (Mach = 3.38) 46

4.21 Dissociated Oxygen versus

Magnetic Field Strength (Mach = 3.38) 46

4.22 Entropy versus Magnetic Field Strength (Mach = 3.38) 47

4.23 Accelerator Performance (Mach = 3.38, 16 Tesla Field) 49

4.24 Temperature versus Magnetic Field Strength (Angle = 0.9°) 50

4.25 Dissociated Oxygen versus

Magnetic Field Strength (Angle = 0.9°) 50

4.26 Entropy versus Magnetic Field Strength (Angle = 0.9°) 51

4.27 Accelerator Performance (Angle = 0.9°, 12 Tesla Field, 2.0% K) .. 52

4.28 Accelerator Performance (Angle = 0.9°, 16 Tesla Field, 0.5% K) .. 54

4.29 Accelerator Performance (Mach 25 Simulation) 57

4.30 Accelerator Performance (Mach 15 Simulation) 59

LIST OF ABBREVIATIONS

Arnold Engineering Development Center .... AEDC

High Density Accelerator Program at AEDC .... HIRHO

Low Density Accelerator Program at AEDC .... LORHO

Magnetohydrodynamic .... MHD

National Aeronautics and Space Administration .... NASA

National Aero-Space Plane .... NASP

Pressure Ratio of Upstream Nozzle .... PCP

United States Air Force .... USAF

LIST OF SYMBOLS

A	Duct Cross-Sectional Area (square meter)
B	Magnetic Field Flux Density (Weber/square meter)
D	Hydraulic Diameter (meter)
E	Electric Field (Volt/meter)
E_d	Electric Field of Plasma to Electrode Voltage Drop (Volt/meter)
h	Static Enthalpy (MegaJoule/kilogram)
H	Total Enthalpy (MegaJoule/kilogram)
J	Current Density (amps/square centimeter)
m	Mass Flow Rate (Kilogram/second)
P	Pressure (atmosphere)
R	Gas Constant
T	Temperature (degrees Kelvin)
s	Entropy (kiloJoule/kilogram degrees Kelvin)
q	Dynamic Pressure (pounds/square foot)
q_w	Wall Heat Transfer (Watt/square meter)
u	Velocity in x-direction (meter/second)
x, y, z	Right-Hand Coordinate System
X_O	Mole Fraction of Dissociated Oxygen
ρ	Density (kilogram/cubic meter)
σ	Conductivity (siemens/meter)

1.0 INTRODUCTION

1.1 The History of MHD Acceleration for Hypersonic Simulation

Magnetohydrodynamics (MHD) has been defined as the science of the motion of electrically conducting fluids under the influence of magnetic fields. Faraday produced the first documented account of such interactions in 1832. He believed that the motions of the oceans might account for the deviations in the earth's magnetic field. Very little laboratory work could be done in the 1830's due to the lack of any suitable conducting fluid, thus the science remained vastly theoretical.

In 1919, an engineer named Petersen proposed the use of an ionized gas as an armature and was granted a U.S. patent for his design of a MHD generator. The principle of his generator was to pass the ionized gas through a magnetic field. The MHD interaction would then produce an electric field orthogonal to both the flow of the fluid and the magnetic field. By placing electrodes transverse to the generated electric field, the electricity could be harnessed for use. For a simple MHD generator the interaction can be described by the vector equation $\mathbf{E} = \mathbf{u} \times \mathbf{B}$, where $\mathbf{u}$ is the velocity of the conducting fluid, $\mathbf{B}$ is the applied magnetic field, and $\mathbf{E}$ is the electric field produced. Figure 1.1 details a schematic of a simple MHD generator, with an imposed conducting flow and magnetic field producing an induced current across the channel.

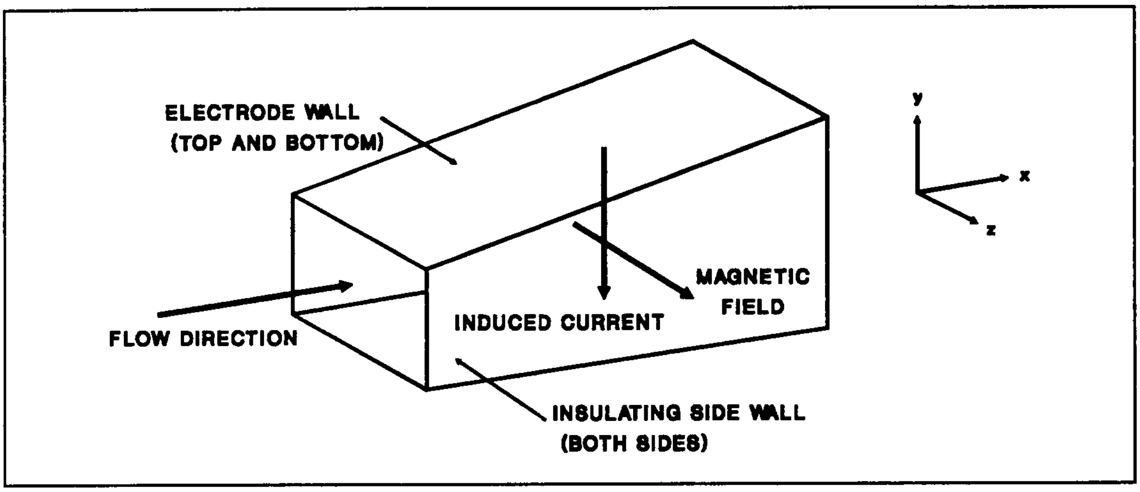

Figure 1.1 : Simple MHD Generator

Following World War II there was a boom in applied science research. One idea was to use MHD acceleration to produce high Mach number wind tunnels for simulation of hypersonic flight. MHD acceleration is merely another form of the same MHD interaction. Instead of using the generated electric field as with the MHD generator, an electric field is applied orthogonally to the velocity of the conducting fluid and the magnetic field in a direction opposing the generated field.

As with the generator, $\mathbf{u} \times \mathbf{B}$ creates an electric field in the y-direction, however, there now exists an applied electric field ($\mathbf{E}_{app}$) in the opposite direction. Thus the total electric field is $\mathbf{E}_{app} + \mathbf{u} \times \mathbf{B}$, which can be converted to a current density $\mathbf{J} = \sigma(\mathbf{E}_{app} + \mathbf{u} \times \mathbf{B})$ where σ is the conductivity. It can be seen in figure 1.2 that the electric field, and hence the current, is orthogonal to the magnetic field, this produces the $\mathbf{J} \times \mathbf{B}$ body force which is the basis of MHD acceleration. The $\mathbf{J} \times \mathbf{B}$ body force adds kinetic energy directly to the flow, thus increasing the overall velocity with a minimal increase in static temperature and pressure.

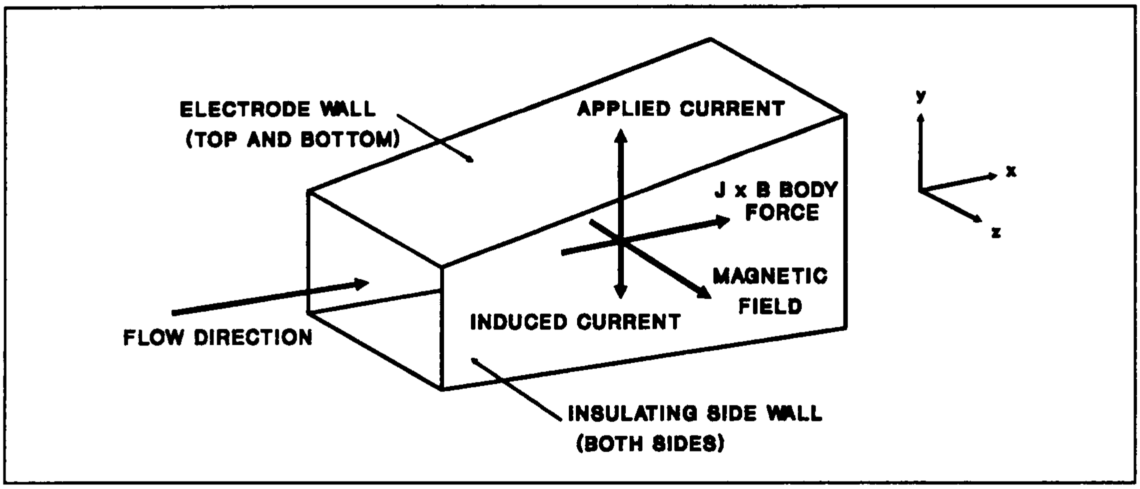

Figure 1.2 : Simple MHD Accelerator

Research of hypersonic flight vehicles in the 1960's fostered a need for hypersonic-environment simulation. Hypersonic velocities are defined as those velocities that exceed Mach 5. Current facilities available can test large structures or propulsion systems for flight to about Mach 7, but not beyond (Richey and McKinney, 1993). Due to the extreme total pressures needed to simulate this flow field, it is not possible, because of material limits, to pump a reservoir with air to the necessary pressure for an expansion to the right conditions. One alternative examined was to use MHD augmentation of arc-heated and shock driven-tube facilities. The MHD accelerator is able to add directed energy to the flow which can increase the velocity without increasing the static pressure (Ring, 1964). The most significant research was performed at the USAF Arnold Engineering Development Center (AEDC) and the NASA Langley Research Center. Unfortunately, the programs were terminated before any full scale prototype facilities were developed. AEDC performed major research and testing in the

HIRHO and LORHO programs developed during this time. The AEDC reports provided a key historical reference for the UTSI study.

Some interest in the MHD accelerators persisted into the 1970's as research groups investigated reentry vehicle development. More interest, however, was directed toward new programs in MHD power generation as a result of the concern for energy. Although the accelerator operates under a more extreme environment, the large database of generator technology will greatly aid the development of an accelerator program.

In the mid-1980's, hypersonic flight vehicle research and hypersonic air-breathing propulsion development renewed the interest in MHD acceleration. The National Aero-Space Plane (NASP) research needs a means to perform wind tunnel testing at up to Mach 25 conditions. It was for this reason that UTSI began researching the MHD accelerator as a means to provide the necessary test conditions for the NASP.

During the last thirty years, Russia has also been investigating the capabilities of MHD augmented hypersonic ground test facilities. An operational hypersonic wind tunnel has been built and many characteristics of the flow field have been studied. The Russian facility is very similar to the design investigated at UTSI. An arc-heater is used to pre-heat the air which is then seeded with NaK, an alloy of Sodium and Potassium. The accelerator channel used is a segmented Faraday-type with an adjustable power supply system. The channel is fairly small however, with a 2 cm x 2 cm cross-section and mass flow rates of 10-50 gm/sec.

The Russian wind tunnel proves that the facility UTSI proposed can be implemented to produce a functional hypersonic ground test facility.

1.2 A Brief Summary of the UTSI Investigation

This thesis continues the investigation conducted by the University of Tennessee Space Institute (UTSI) in the report Potential Application of Magnetohydrodynamic Acceleration to Hypersonic Environmental Testing (Crawford, Chapman, and Rhodes, 1990). The goal of this report was to identify, by theoretical analysis, the performance potential of MHD generator and hot gas generator combinations for which satisfactory and credible design, construction, and operating characteristics could be predicted. The report studied this potential for the Mach 10 to 25 range of hypersonic flight simulation.

The previous UTSI report presented a list of conclusions and recommendations that summarized the results of the study. This summary was divided into three parts; channel design trade off study conclusions, flow expansion and simulation conclusions, and recommendations. Included in this section are the results which are important to the topics being discussed in this paper. Only a partial list of the results is included, focusing on the results pertinent to this thesis.

- A single channel geometry and primary magnet may provide a large range of high Mach number simulation (15-25) by varying only the applied electrode power and downstream nozzle area ratio.

- Magnetic field strength is paramount for acceleration efficiency and improves aerodynamic simulation capability at free-stream conditions.
- Required seed density is determined by inlet conductivity limits and gas generator performance. Seed density of 0.5 to 1.0 percent potassium by weight was found to be adequate for most accelerator calculations made during the study.
- For an MHD accelerator of fixed mass flow and performance, inlet pressure controls channel cross-sectional area, electrode current density, and wall heating rates.
- For a given electrode current density, a reduction in operating pressure results in an increase in cross section area and a reduction in channel length. Holding the geometry constant, the reduction in pressure would reduce the necessary current density.
- Velocity was well simulated because total enthalpy was correctly simulated and the kinetic energy term dominates.

1.3 Investigation Goals

Although UTSI has shown that there is some promise for MHD accelerators in this application, there were some who questioned certain aspects of the results. Four main objections were expressed by NASA and USAF hypersonic advocates about the previous report. The criticisms of the report are:

- The inclusion of seed in the air does not provide true simulation
- The static temperatures in the test section are slightly high.
- Oxygen disassociation is about twice that which would be expected at the engine inlet.
- There does not seem to be a configuration that even approaches the free-stream test conditions at high Mach Number.

The intent of this thesis is to carry out further research to answer some of the questions that were brought up regarding the past investigation. The topics which are addressed in this paper are:

- Reducing the amount of seed needed for MHD interaction
- Reducing the temperatures in the test section for the direct connect case to within reasonable limits.
- Reducing the oxygen disassociation to that which would be expected at the engine inlet.

1.4 Investigation Limits

In order to achieve the investigation goals, three variables in the MHD accelerator configuration are studied. By manipulating these three variables, the configuration which best satisfies the primary issues of this thesis will be determined. The variables of study are:

- The design of the upstream nozzle to vary the entrance pressure.
- The divergence angle of the accelerator channel walls.
- The strength of the magnetic field.

The investigation of these three variables should produce better understanding of the effects which each produces on the test environment conditions. Additionally, the amount of seed needed will be examined as an overall variable. With the results of these studies, a test configuration will be developed that will attempt to simultaneously meet the three investigative goals of this paper.

1.5 Method of Development

To correctly address the goals of this investigation some background work must first be presented. Chapter 2 of this report will detail the simulation requirements necessary for the hypersonic environment. Following this, Chapter 3 details the assumptions made in order to model the direct connect MHD accelerator hypersonic wind tunnel. This chapter includes the models used for calculations upstream, downstream, and within the MHD accelerator.

Chapter 4 details the investigation itself, with trade-off studies focusing on each of the investigation variables. The first section sets forth the base accelerator case as used in the previous UTSI investigation. Section 4.2 considers the variation of entrance pressure in the accelerator. Section 4.3 determines an optimum ratio of the accelerator entrance and exit areas. Section 4.4 details the effect of magnet field strength on the efficiency of the MHD accelerator. Section 4.5 develops the best accelerator configuration based on the individual studies performed. Finally section 4.6 tests the results for other Mach numbers.

The study is summarized in Chapter 5 with the conclusions found in the various trade-off studies. It is noted here that while potassium cannot be eliminated, it can be reduced, and the other concerns minimized. Finally, recommendations are made for additional investigations, in order to improve the MHD accelerator solution even further.

2.0 SIMULATION REQUIREMENTS

The development of the National Aero-Space Plane (NASP) is the driving force behind the MHD accelerator hypersonic wind tunnel. The NASP is to be a single stage aircraft with a combined cycle airbreathing propulsion system, which will take off horizontally, be able to attain orbit, and return safely to earth. The NASP flight trajectory is such that the aircraft will accelerate from low subsonic Mach numbers, through hypersonic flight, and up to a peak Mach number of 25 at an altitude of 250,000 feet.

One of the most important areas of research for the NASP is ground testing for the propulsion system, since this is the first attempt to operate a large scale hydrogen combustion system in both subsonic and supersonic modes with a single engine. Certain parameters exist in the real world situation that must be duplicated near exactly in the testing environment. Because the specific goal of this design study is to develop a test facility for hypersonic propulsion testing, the necessary parameters for an acceptable simulation need elucidation.

2.1 Hypersonic Flight Envelope

To accurately model a hypersonic flight vehicle, certain simulation and non-dimensional parameters must be known. Total enthalpy, static temperature, static pressure, entropy, Mach number, Reynolds numbers, Prandtl number, and the associated thermodynamic properties are the important parameters. Perhaps the most important parameter is the total enthalpy, because it assures that the total temperature is duplicated (Ring, 1964).

To attain values for the parameters, a specific range of investigation must be determined. Figure 2.1 shows a typical hypersonic flight vehicle envelope plotted as a graph of altitude versus velocity. The upper limit of the envelope is the constant dynamic pressure (q) line at 500 psf, which is determined by the lift or propulsion limits. The lower limit is determined by dynamic pressure or heating limits, and is at the 2000 q line. Further restrictions for an air-breathing powered vehicle are combustion and heat transfer limits, shrinking to between the 500 q and 1000 q lines. For this investigation, all calculations have been performed with properties commensurate with the 1000 q line.

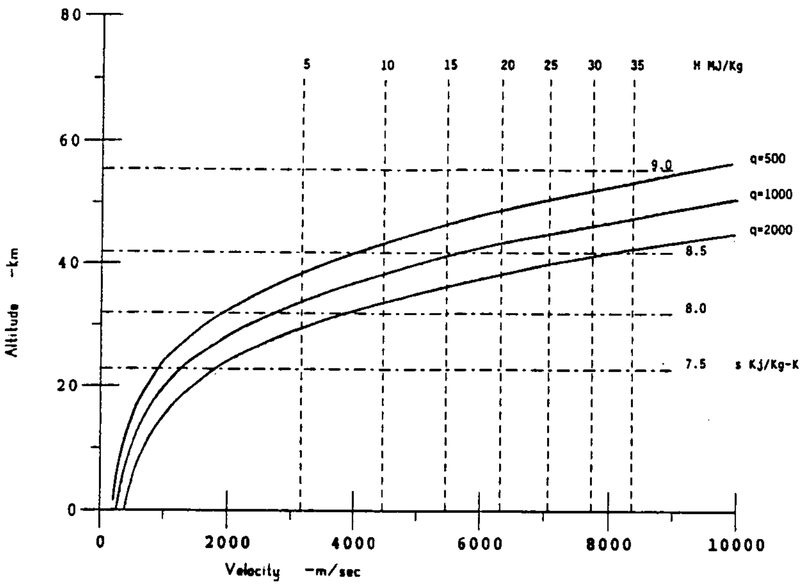

Figure 2.1 : Hypersonic Flight Envelope

Source: Crawford, R.A., Chapman, J.N., and Rhodes, R.P. "Potential Application of Magnetohydrodynamic Acceleration to Hypersonic Environmental Testing." AEDC-TR-90-6, August 1990, page 11.

2.2 True-Air Conditions

When testing the propulsion system, it will be important to measure chemical reaction rates and combustion performances. To correctly simulate hypersonic flight in a test facility, 100 percent true air would have to be used. Air by itself, however, will not ionize to the level necessary for the MHD interaction to occur within a reasonable temperature bound. To obtain sufficient conductivity, the air must be seeded with an easily ionized element or compound. Elemental potassium seems to be the best choice due to its low cost and molecular weight considerations (Crawford, Chapman, and Rhodes, 1990).

One of the criticisms of the original study by NASA and USAF is the presence of potassium seed in the air. To approach the true-air condition, the amount of seed used must remain at a minimum. Early investigations found that 0.5 to 2.0 percent potassium was found to be adequate, depending on the inlet conductivity and gas generator performance. Seeding levels below 0.5 percent potassium create the possibility of electrode arcing at the lower conductivity levels, and should be avoided (Crawford, Chapman, and Rhodes, 1990). Figures 2.2 and 2.3 show the difference in conductivity and air seeded with 2.0 and 0.5 percent potassium at various temperatures and pressures. The graphs show that reducing the temperature reduces the conductivity, while reducing the pressure increases the conductivity. Most calculations throughout this thesis have been made for both the 2.0 and 0.5 percent potassium cases.

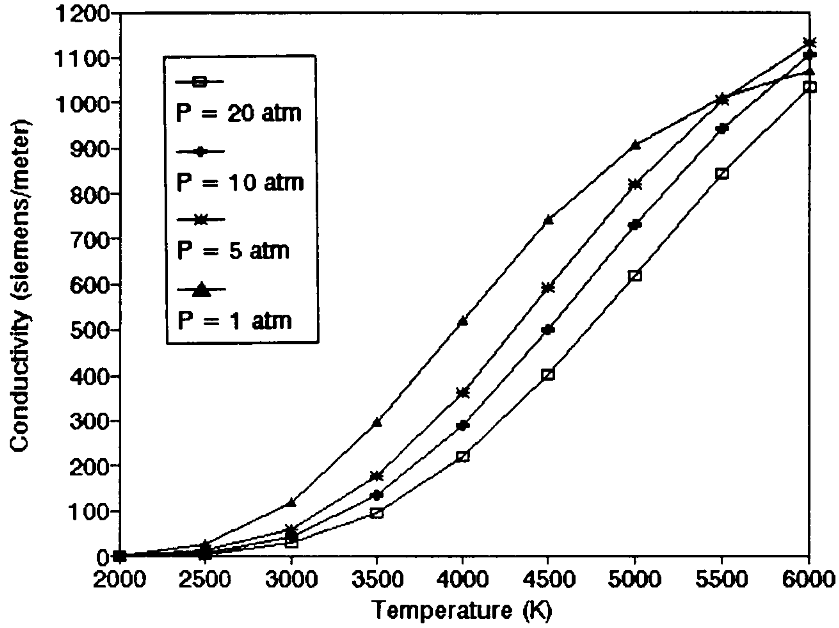

Figure 2.2 : Conductivity of Air with 2.0 Percent Potassium

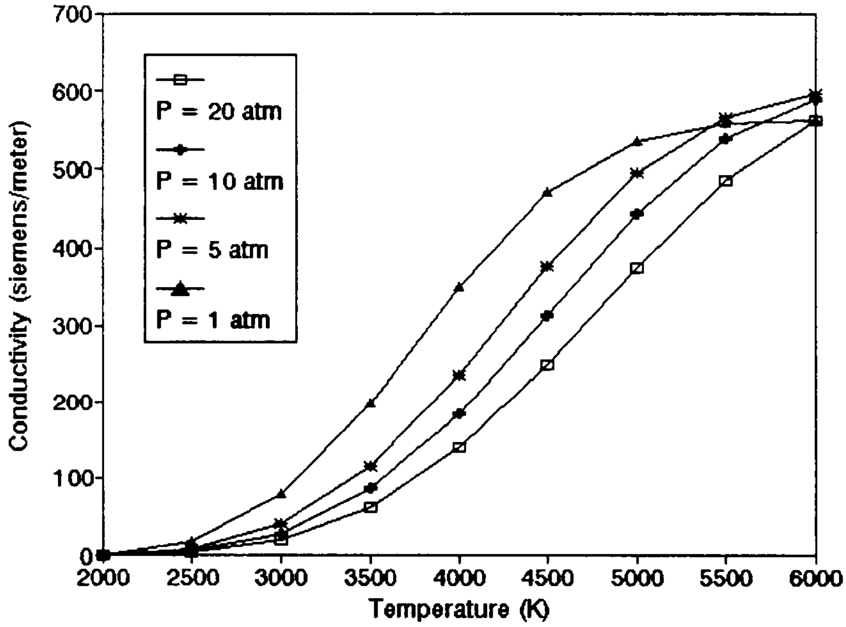

Figure 2.3 : Conductivity of Air with 0.5 Percent Potassium

2.3 Direct-Connect Propulsion Testing

Figure 2.4 shows the flight regime in terms of enthalpy versus entropy for various locations on the aircraft's body for the q = 1000 psf flight path. To design the NASP, there are three hypersonic flight vehicle simulation conditions which are shown on the figure. The three simulation requirements are: (1) free stream, (2) cowl lip, and (3) combustor inlet envelope. The free stream represents the condition of the air which is undisturbed by the body or form of the aircraft, such as at the leading edge of the aircraft. In the other two regimes, the air has been taken to be compressed by bow shock waves to produce a lower Mach number,

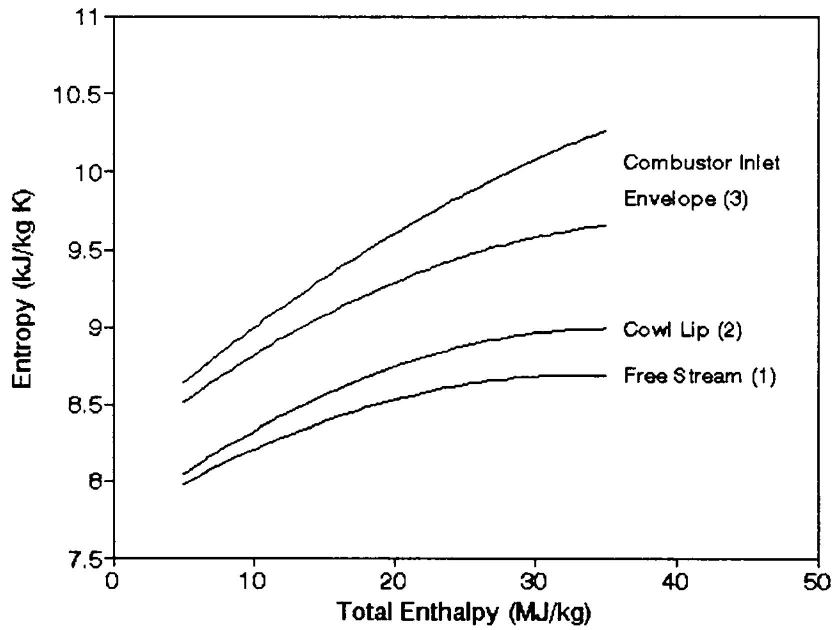

Figure 2.4 : Combustor Test Conditions for q = 1000 psf

a higher pressure, and a higher temperature than at free stream conditions. The actual simulation regions will depend on the aerodynamics of the aircraft. The regions shown on the figure were estimated from typical values of NASP-type inlet losses (Waltrup, Billig, and Stockbridge, 1987).

The combustor inlet is the easiest region to simulate due to the lower Mach number, higher pressure, and higher temperature. These conditions are closer to the results obtained in the first UTSI report on MHD acceleration than the free stream conditions. To simulate the condition of air already compressed by the aircraft body, propulsion testing will be performed in direct-connect mode. That is, the air-breathing hypersonic propulsion system will be directly in line with the MHD augmented wind tunnel. This will produce very accurate simulation with the only property not exactly reproduced being the gas species concentrations.

3.0 MODEL OF DIRECT-CONNECT MHD ACCELERATOR HYPERSONIC WIND TUNNEL

Figure 3.1 shows a conceptual drawing of a direct-connect hypersonic flow simulation facility. The facility is made up of the arc heater, seed injector, upstream nozzle, accelerator channel, downstream nozzle, combustor module, diffuser, and exhaust system. This chapter describes the components of the system, and how they are modeled in this investigation. The facility is divided into three parts for this description; the upstream (components preceding accelerator), the MHD accelerator channel, and the downstream (components following the accelerator).

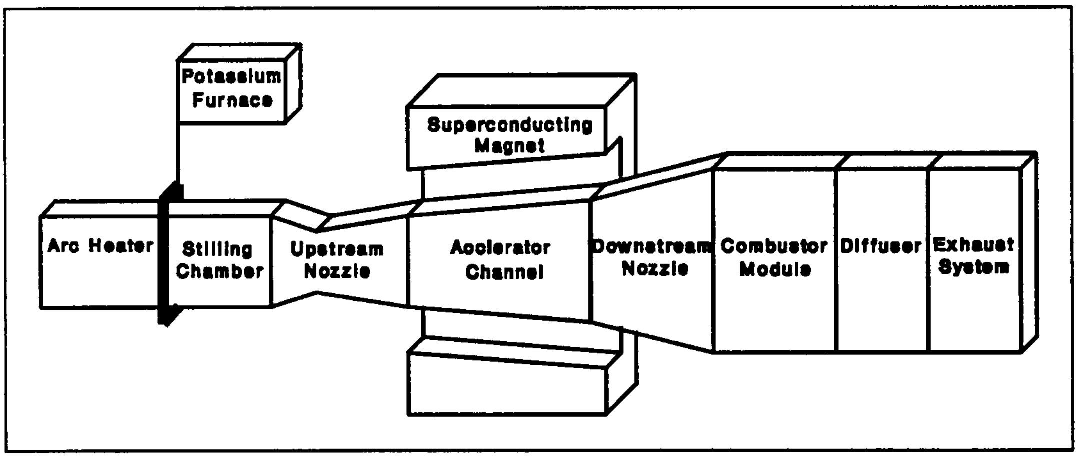

Figure 3.1 : MHD Augmented Direct-Connect Simulation Facility

3.1 Upstream Simulation

The upstream portion of the MHD augmented wind tunnel includes all components that precede the accelerator channel. There are three main upstream components in the hypersonic flow simulation facility: the arc heater, the seed injector system, and the upstream nozzle. The following is a description of the model used for each component and assumptions made.

For the investigation, an arc heater was chosen that produces heated air at 200 atm with a mass flow rate of 22.1 kg/sec. The heat transfer limits of the arc heater can be expressed as a line of constant $HP^{1/2}$ = 93.06 MJ/kg atm$^{1/2}$. For all calculations the following arc heater exit conditions were assumed:

$$H = 6.65 \text{ MJ/kg},\quad T = 4751 \text{ K},\quad P = 200 \text{ atm},\quad s = 8.86 \text{ kJ/kg K}$$

This arc heater performance is beyond the capability of any current equipment, but is believed to be representative of that achievable with arc heater technology without increasing the heat transfer limits.

The seed injector system is made up of two parts: the potassium furnace and the stilling chamber. The potassium in the furnace is maintained under pressure and heated until the potassium is vaporized. The vaporized potassium seed is then injected into the stilling chamber where it mixes with the air exiting from the arc heater. In this investigation it is assumed that the seed mixes uniformly with the arc heated air to produce a homogeneous composition.

The final upstream component is a contoured converging-diverging nozzle to accelerate the flow to the desired accelerator entrance velocity. The nozzle length needs to be minimized to reduce heat and friction losses. To model the nozzle expansion the fortran program NASA SP-273 is used. NASA SP-273 is a thermodynamic equilibrium code, modified to include the calculation of electrical transport properties. The thermodynamic input variables are taken to be the exit values of the arc heater. The chemical species are input as air mixed with either 2.0 or 0.5 percent potassium by weight, depending on the test case. The program is run using the rocket performance option and assumes thermochemical equilibrium and no losses during the expansion. The flow is expanded to the pressure or Mach number desired for the accelerator inlet.

3.2 MHD Accelerator Simulation

The general accelerator to be used to augment the hypersonic wind tunnel was designed previously in work done at UTSI. The accelerator is a square duct with construction similar to a segmented electrode Faraday MHD generator. The electrode walls consist of 127 pairs of electrodes and interelectrode insulators. The electrodes are highly-cooled copper, 2.5 cm wide and separated by 0.3 cm boron nitride interelectrode insulators. The entire accelerator channel is taken to be located inside the bore of a superconducting magnet.

To model the performance of the MHD accelerator, a one-dimensional accelerator code was written and has been used routinely by the UTSI MHD group. The code accounts for wall heat flux, wall friction, and variable thermodynamic properties.

The following assumptions were used in the accelerator model:

- The flow is one-dimensional and uniform in a plane perpendicular to the flow.
- Induced magnetic fields are negligible.
- The gas is in chemical and thermodynamic equilibrium.
- The gas is homogenous in species concentration and thermodynamic properties.
- The plasma-to-electrode voltage drops are proportional to applied voltage.
- The applied magnetic field is uniform and one-dimensional.

The following input data is required by the code:

- Entrance temperature and pressure
- Wall temperature
- Mass flow rate
- Entrance area and axial profile
- Maximum magnetic field and profile
- Wall roughness height
- The electrical boundary layer loss factor

- Channel length and computational step size
- Channel loading and maximum J_y if desired

The one-dimensional equations used in the code are:

Momentum Equation:

$$\rho u \frac{du}{dx} + \frac{dP}{dx} = -J_y B - 4\frac{\tau_w}{D}$$

Energy Equation:

$$\rho u \frac{dh}{dx} + \rho u^2 \frac{du}{dx} = J_y E_y + 4\frac{q_w}{D}$$

Continuity Equation:

$$\rho u A = \dot{m}$$

Ohm's Law:

$$\vec{J} \cdot \vec{E} = \frac{J^2}{\sigma} - J_y u B(1 - \frac{E_d}{uB})$$

Equation of State:

$$P = \rho R T$$

Thermodynamic State:

$$h = h(P,\ T)$$
$$R = R(P,\ T)$$

These equations can be manipulated to derive the following two equations:

$$\left(\frac{1}{R}\frac{\partial R}{\partial T} + \frac{1}{T}\right)\frac{dT}{dx} + \left(\frac{1}{R}\frac{\partial R}{\partial P} - \frac{1}{P} - \frac{1}{\rho u^2}\right)\frac{dP}{dx} = \frac{1}{A}\frac{dA}{dx} - \frac{J_y B}{\rho u^2} - \frac{4\tau_w}{\rho u^2 D}$$

$$\left[\frac{1}{u^2}\frac{\partial h}{\partial T} + \frac{1}{R}\frac{\partial R}{\partial T} + \frac{1}{T}\right]\frac{dT}{dx} + \left[\frac{1}{u^2}\frac{\partial h}{\partial P} + \frac{1}{R}\frac{\partial R}{\partial P} - \frac{1}{P}\right]\frac{dP}{dx} = \frac{1}{A}\frac{dA}{dx} + \frac{\vec{J}\cdot\vec{E}}{\rho u^3} + \frac{4q_w}{\rho u^3 D}$$

The above two derived equations can be used with the continuity equation to form a set of three equations with four unknowns (u, P, T, A). If any one of these variables are known, the set of equations can be solved to find the other three. In this study, the accelerator channel geometry is chosen to be specified in all cases, therefore the area is known with respect to the accelerator length. The other three variables can then be determined by numerical integration of the governing differential equations. In all calculations J_y is assumed constant at all points in the channel. The losses are accounted for in a global sense and thermochemical equilibrium is assumed.

3.3 Downstream Simulation

The downstream portion of the MHD augmented wind tunnel consists of four components. They are the downstream nozzle, the scramjet combustor module, the diffuser, and the exhaust system. As this paper is concerned only with obtaining the correct test conditions at the combustor module, the diffuser and exhaust systems are not considered. The inlet to the scramjet combustor module is assumed to have a homogeneous flow field.

The downstream nozzle expands the accelerated air from the accelerator exit conditions to the static pressure at the combustor inlet. The expansion is modeled with a Kinetic Expansion program that is derived from the LAPP code (Mikatarian, Kau, and Pergament, 1972). The expansion is calculated using finite rate chemical kinetics. For the expansion, viscous loses and wall heating are not considered.

4.0 MHD ACCELERATOR TRADE-OFF STUDIES

Within this chapter several design parameters of the MHD augmented hypersonic wind tunnel are studied to develop an optimum accelerator channel design. First the baseline channel and operating conditions are described in detail. This is the same baseline design used in the UTSI report. The next sections present trade-off studies for accelerator channel inlet Mach number, accelerator channel area ratio, and magnetic field strength for the baseline case of Mach 20 simulation. Finally the optimum accelerator channel configuration is developed and results are presented for other Mach numbers.

4.1 Baseline Channel Design

The baseline test case developed for the previous UTSI investigation was selected at Mach 20 along the q = 1,000 psf flight envelope line. The proposed arc heater exit condition, a reasonable estimate for current technology, is inadequate in meeting the desired test condition. To attain the target conditions, the flow is passed through the accelerator channel to produce a total enthalpy of 22.65 MJ/kg at the accelerator exit. Table 4.1 includes the baseline channel design for the accelerator and the performance results produced from this configuration. Because the downstream nozzle was assumed lossless, the total enthalpy and entropy values from the accelerator exit are equivalent to the test

Table 4.1 : Baseline Accelerator Performance

Parameter	Inlet	Exit
Static Pressure (atm)	20.00	4.14
Static Temperature (K)	3255	4019
Velocity (m/sec)	2298	5665
Density (kg/m^3)	2.149	0.329
Ratio of Specific Heats	1.204	1.189
Conductivity (mho/m)	56.45	317.0
Entropy (kJ/kg K)	8.86	10.06
Total Enthalpy (MJ/kg)	6.61	22.73
Total Pressure (atm)	197.7	4160
Mach Number	2.156	4.602
Current Density (amps/cm^2)	50.00	
Specific Heat Flux (kw/cm^2)	8.08	
Total Power (MW)	456	

chamber conditions. Figure 4.1 shows the accelerator simulation results on the enthalpy versus entropy plot and the relationship to the combustor inlet envelope.

One of the conclusions of the UTSI paper is that a large simulation envelope can be produced by varying the electrode current. This fact is used to perform the trade-off studies. The various channel parameters are changed for each test case, then the electrode current is adjusted until the design point enthalpy is attained at the accelerator channel exit. The flow is then expanded through the downstream nozzle to the desired combustor module inlet conditions.

The target properties needed to simulate the combustor inlet conditions for the NASP were theoretically calculated by the John Hopkins University Applied Physics Laboratory (1986). These values are designated as "target values" in this

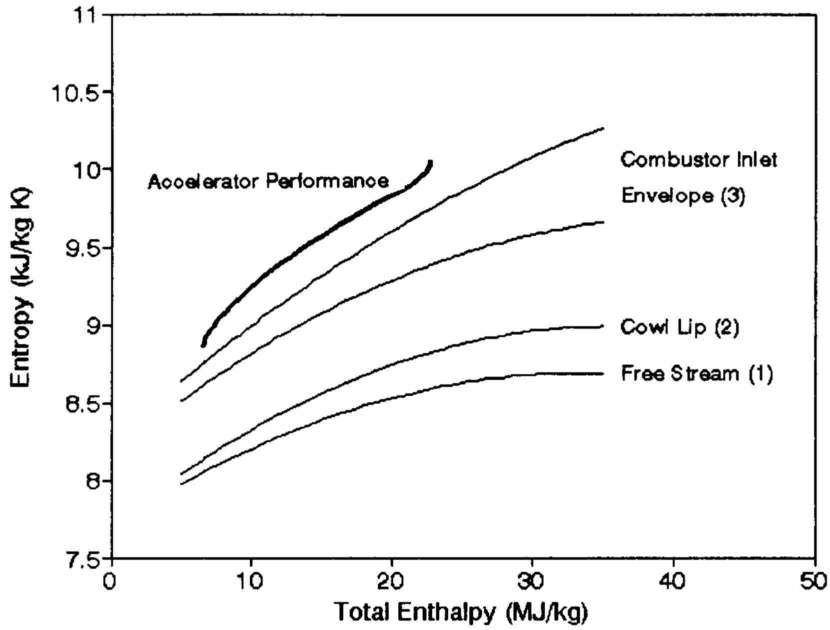

Figure 4.1 : Baseline Accelerator Performance

thesis. For the baseline case of Mach 20 simulation the following target values of static pressure, static temperature, and flow velocity are given:

$$P = 0.50 \text{ atm}, \quad T = 2642 \text{ K}, \quad u = 6008 \text{ m/s}$$

The target values for total enthalpy and entropy are the range of values in the combustor inlet envelope as shown in figure 4.1. A reasonable target value for the mole fraction of dissociated oxygen (X_O) at the combustor inlet is 0.075. In all cases the accelerator is designed to add energy to the flow and increase its total enthalpy to 22.65 MJ/kg which ensures the velocity is well simulated. The flow is subsequently expanded through the downstream nozzle to a pressure of 0.50 +/- 0.01 atms and the values of temperature, entropy, and oxygen dissociation are compared to the target values.

4.2 Accelerator Entrance Mach Number

One method reaching the target combustor inlet values is to optimize the accelerator performance as a function of the amount of expansion from the arc heater. For a fixed arc heater pressure, the flow is expanded to a higher Mach number reducing the static pressure and static temperature. The decreased static temperature will tend to reduce the conductivity of the flow, while the decreased static pressure will tend to increase it. Therefore a trade-off study must be performed to determine the optimum pressure ratio.

The arc heater performance was held constant, so the nozzle inlet pressure is always 200 atm. For the baseline design, the nozzle chosen has a pressure ratio of 10, producing an accelerator entrance Mach Number of 2.16. Since a constant mass flow rate of 22.10 kg/sec is to be maintained, the accelerator inlet conditions determine the entrance area of the accelerator channel. Various entrance conditions were examined using the NASA SP-273 code to vary the inlet/exit pressure ratio, and thus the Mach number, of the upstream nozzle. Table 4.2 shows the nozzle exit conditions, the resulting accelerator inlet and exit areas, and the channel entrance conductivity levels that are produced by the different pressure ratios. It should be noted, there may exist a minimum conductivity required to maintain diffuse current transport, but this limit is unknown.

The calculated nozzle exit conditions are the inlet variables for the accelerator channel calculation. The temperatures, pressures, areas, and

Table 4.2 : Accelerator Channel Inlet Mach Number Cases

PCP	Mach Number	Static Pressure (atm)	Static Temp (K)	Inlet Area (cm^2)	Exit Area (cm^2)	Conductivity 2.0% K (mho/m)	Conductivity 0.5% K (mho/m)
10	2.16	20.00	3238	44.6	118.6	56.45	35.20
15	2.38	13.33	3032	58.5	140.7	41.63	26.21
20	2.53	10.00	2888	77.2	168.7	32.03	20.35
30	2.74	6.67	2688	94.7	194.3	20.60	13.24
40	2.89	5.00	2549	116.2	224.7	14.04	9.21
50	3.01	4.00	2442	136.2	252.2	10.01	6.65
75	3.22	2.67	2252	182.1	313.6	4.78	3.30
100	3.38	2.00	2122	224.0	367.9	2.57	1.86
150	3.61	1.33	1946	300.2	464.0	0.85	0.67
200	3.78	1.00	1827	370.0	549.0	0.35	0.30

conductivities from table 4.2 were used to run the accelerator program. All other input variables have the same value as the baseline test case. Each test case used a different set of input variables and was iterated by adjusting the current density, assumed constant throughout the channel, until the exit total enthalpy was 22.65 MJ/kg to meet the test requirements. The exit static pressure must additionally be constrained to remain above 0.5 atm for all test cases. This is to allow the necessary pressure for the downstream nozzle expansion to the combustor inlet conditions.

The current densities needed to reach the target total enthalpy condition of 22.65 MJ/kg are plotted versus the accelerator inlet Mach numbers for each case in figure 4.2. As the inlet Mach number is increased, the required current density decreases. The values needed to model the baseline case are not significantly

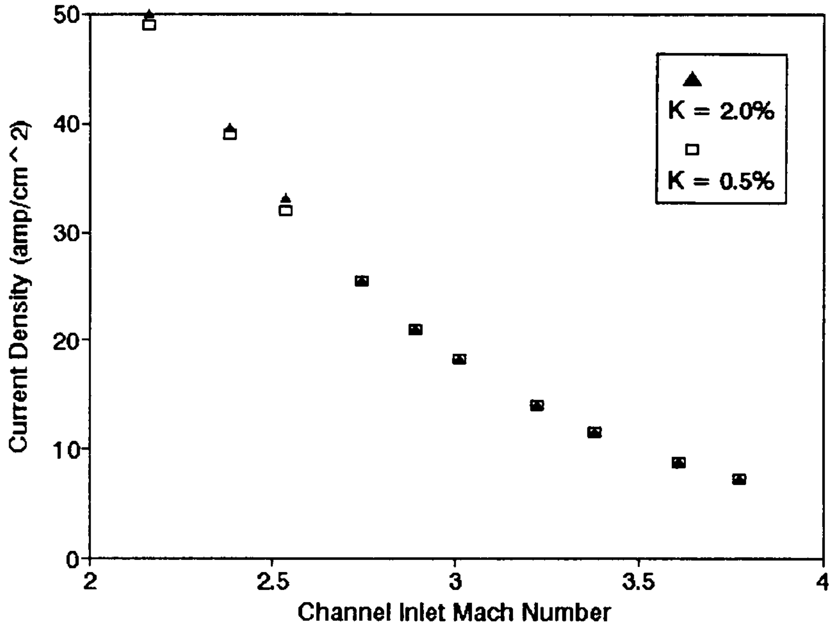

Figure 4.2 : Current Density versus Channel Inlet Mach Number

different for the 2.0 and 0.5 percent potassium seed cases. Because the conductivity is lower with the reduced seed percentage, the 0.5 percent case will require a higher applied accelerating voltage, and consequentially a higher power.

Figure 4.3 shows that by increasing the inlet Mach number, the exit entropy can be significantly reduced. Although the graph indicates that higher inlet Mach numbers may produce lower entropies, the accelerator exit static pressure constraint of 0.5 atms is exceeded at points beyond those shown. It is seen that the entropies of the 0.5 percent seed cases are approximately 1% higher than for the 2.0 percent cases.

Figure 4.4 shows the area ratio of the downstream nozzle versus the accelerator inlet Mach number. The flow was expanded through the downstream

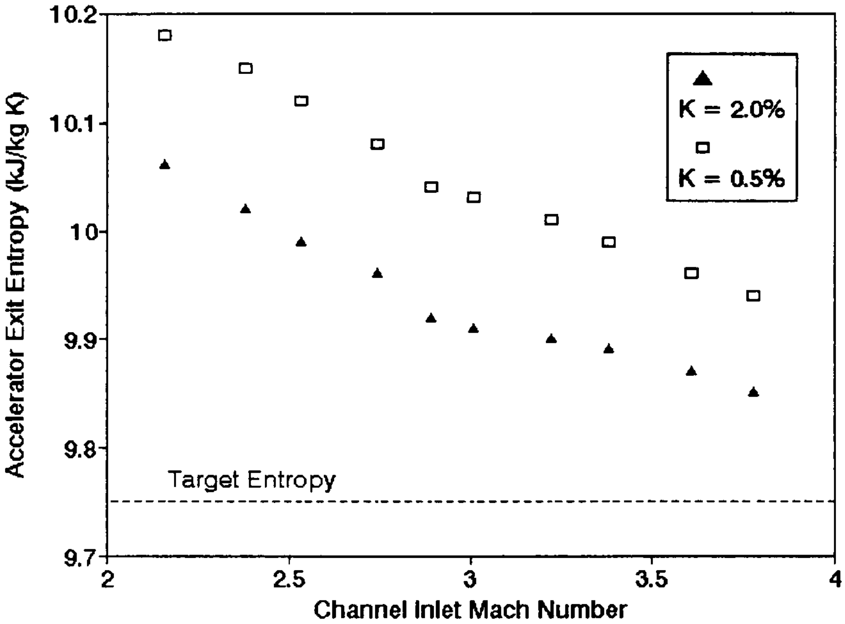

Figure 4.3 : Exit Entropy versus Channel Inlet Mach Number

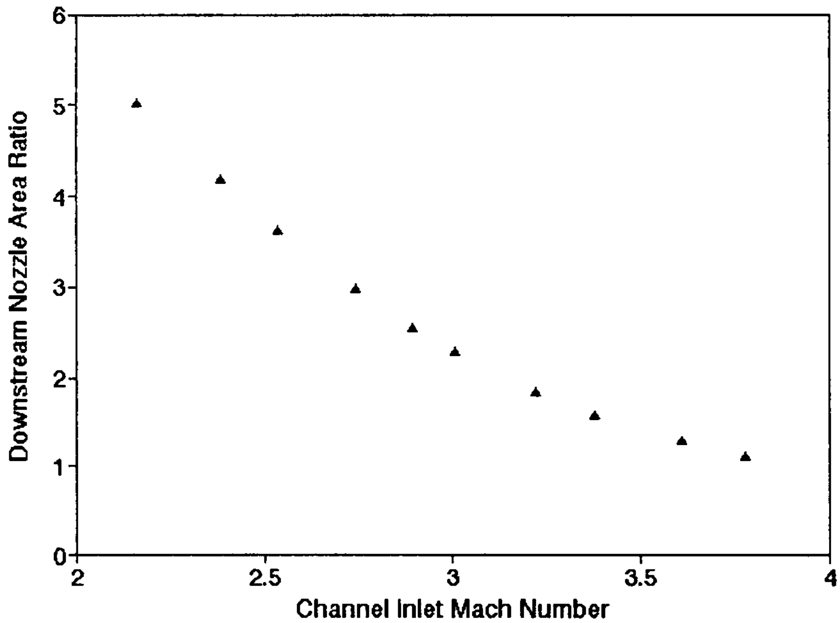

Figure 4.4 : Downstream Nozzle Area Ratio versus Channel Inlet Mach Number

nozzle to the combustor inlet conditions. Each test case was expanded until the static pressure reached 0.5 atm.

The static temperature at the combustor inlet is plotted versus the accelerator inlet Mach number in figure 4.5. The temperature decreases slightly as the inlet Mach number is increased from 2.16 to 2.75, then increases for the remaining cases. The target temperature for the baseline case is 2642 K. A range of the test cases from Mach 2.16 to 3.00 seem to satisfy this condition.

The mole fraction of dissociated oxygen is plotted versus the accelerator inlet Mach number in figure 4.6. As the inlet Mach number increases, the amount of dissociated oxygen decreases. The target value for the mole fraction of dissociated oxygen is 0.075. This condition appears to be satisfied with a Mach of approximately 3.5 at the channel entrance.

The best test case produced by varying the accelerator inlet Mach number seems to be when the inlet Mach number is 3.01. This case satisfies the temperature condition, reduces the entropy, and lowers the amount of dissociated oxygen by 30% from the baseline case. The combustor inlet values of static temperature, oxygen dissociation and entropy for this case are:

$$T = 2663 \text{ K}, \quad X_O = 0.1080, \quad \text{and } s = 9.93 \text{ kJ/kg K}$$

It is noted that this is not a perfect solution, since the amount of dissociated oxygen is still slightly high. Table 4.3 gives the performance results for the Mach 3.00 case. The performance results of this case are plotted on the entropy versus total enthalpy map in figure 4.7.

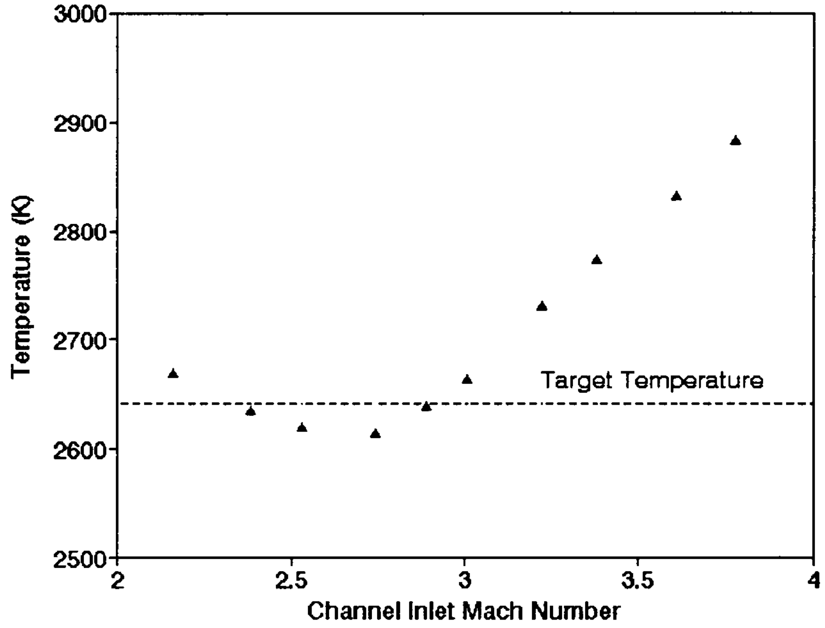

Figure 4.5 : Temperature versus Channel Inlet Mach Number

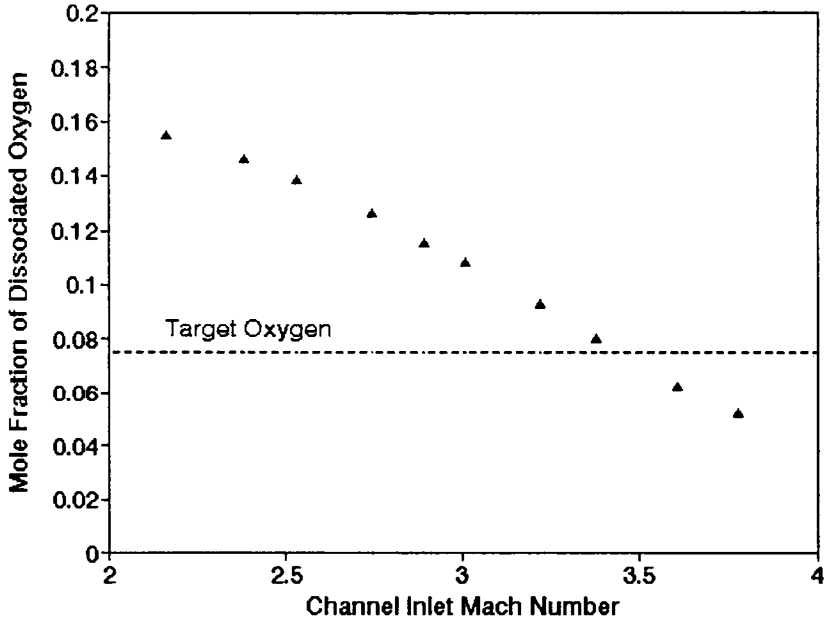

Figure 4.6 : Dissociated Oxygen versus Channel Inlet Mach Number

Table 4.3 : Accelerator Performance (Inlet Mach = 3.01)

Parameter	Inlet	Exit
Static Pressure (atm)	4.00	1.53
Static Temperature (K)	2455	3425
Velocity (m/sec)	2820	5904
Density (kg/m^3)	0.576	0.149
Ratio of Specific Heats	1.245	1.167
Conductivity (mho/m)	10.01	303.3
Entropy (kJ/kg K)	8.87	9.91
Total Enthalpy (MJ/kg)	6.63	22.45
Total Pressure (atm)	178.0	7866
Mach Number	3.011	5.362
Current Density (amps/cm^2)	18.25	
Specific Heat Flux (kw/cm^2)	3.44	
Total Power (MW)	417	

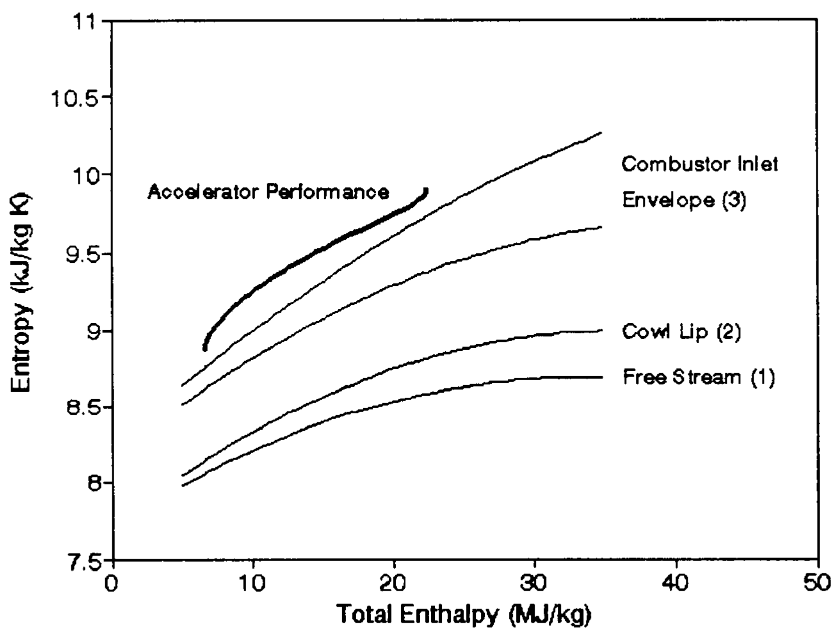

Figure 4.7 : Accelerator Performance (Mach = 3.01)

4.3 Accelerator Channel Divergence Angle

The geometry of the proposed accelerator channel is a duct with an increasing square cross section. The baseline channel design assumed a channel divergence of 0.335 degrees on each wall. The channel has a 44.75 cm^2 inlet area and a 118 cm^2 exit area. Here the effect of changing the wall divergence angle is examined. The inlet area and length of the channel are held constant, so changing the divergence angle only affects the exit area. The calculations were done assuming a square cross section the entire length of the channel. Table 4.4 shows the calculated exit areas for the divergence angles looked at.

The accelerator channel exit areas from table 4.4 were used as input values for the accelerator code, with all other input values, including channel inlet Mach

Table 4.4 : Channel Divergence Angle Input Cases

Divergence Angle (degrees)	Exit Area (cm^2)
0.335	118.4
0.400	136.7
0.500	167.7
0.600	201.6
0.700	238.7
0.800	279.2
0.900	322.6
1.000	369.0
1.100	419.0
1.200	471.8

number and magnetic field strength remaining the same as in the baseline case. In all cases the exit static pressure remained above 0.50 atms in order to be able to expand the flow to the combustor inlet conditions. The accelerator code was run and the current density adjusted until the baseline total enthalpy value of 22.65 MJ/kg was met for each divergence angle. The values of current density are plotted versus the divergence angle in figure 4.8. The required current density decreased as the accelerator divergence angle increased. The values of current density for the 2.0 and 0.5 percent potassium cases are not significantly different.

The results of final entropy values are plotted in figure 4.9 versus channel divergence. Increasing the divergence angle from 0.335° to 1.2° the exit entropy reduces by 2.3% in the 2.0 percent potassium seed case and by 2.5% in the 0.5 percent potassium seed case. The values for entropy of the 0.5 percent potassium case are approximately 1% higher than in the 2.0 percent case.

The exit flow of the accelerator channel was then expanded through the downstream nozzle to the combustor inlet conditions for each case. The flows were expanded until the static pressure reached 0.5 atm. Figure 4.10 shows that the downstream nozzle area ratio decreases as the channel divergence angle increases. Figures 4.11 and 4.12 present the properties after the expansion.

Figure 4.11 shows the static temperature at the combustor inlet plotted versus the divergence angle. The temperature decreases as the divergence angle increases until the divergence angle reaches 0.6°, after that point the temperature increased with the channel divergence. The range of divergence angles from

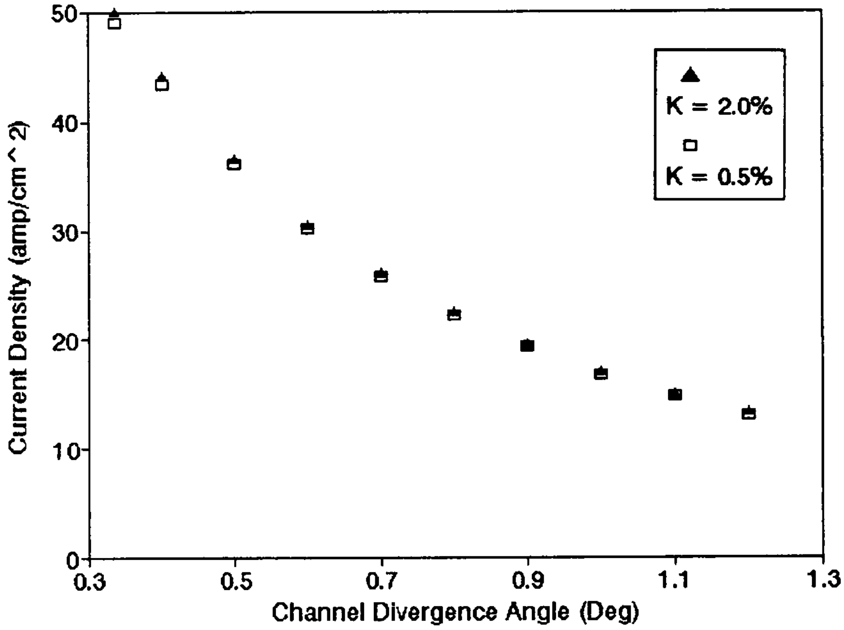

Figure 4.8 : Current Density versus Channel Divergence Angle

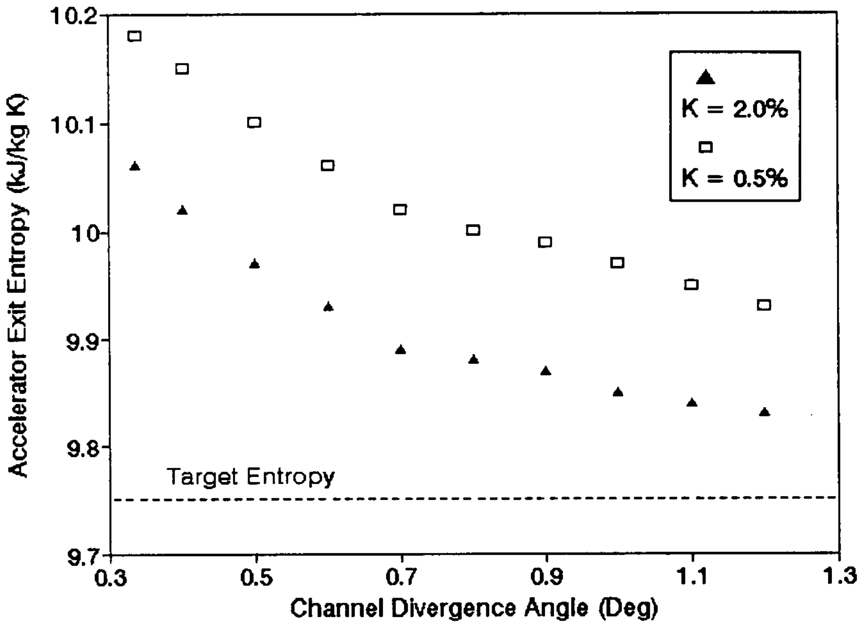

Figure 4.9 : Exit Entropy versus Channel Divergence Angle

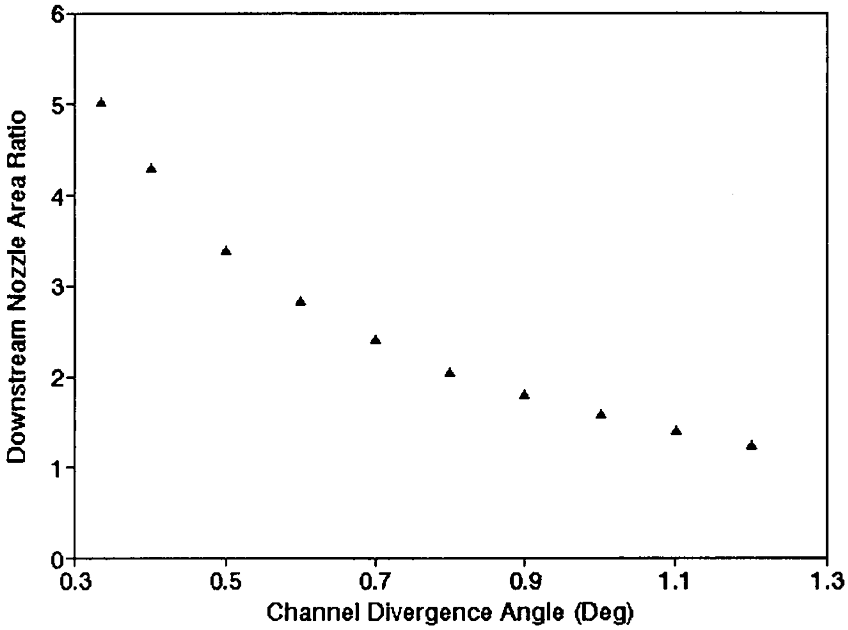

Figure 4.10 : Downstream Nozzle Ratio versus Channel Divergence Angle

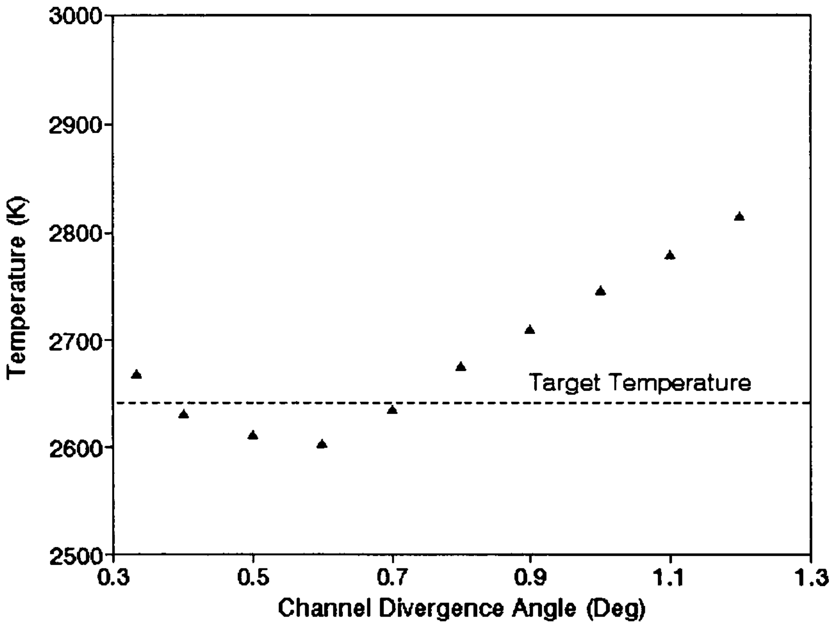

Figure 4.11 : Temperature versus Channel Divergence Angle

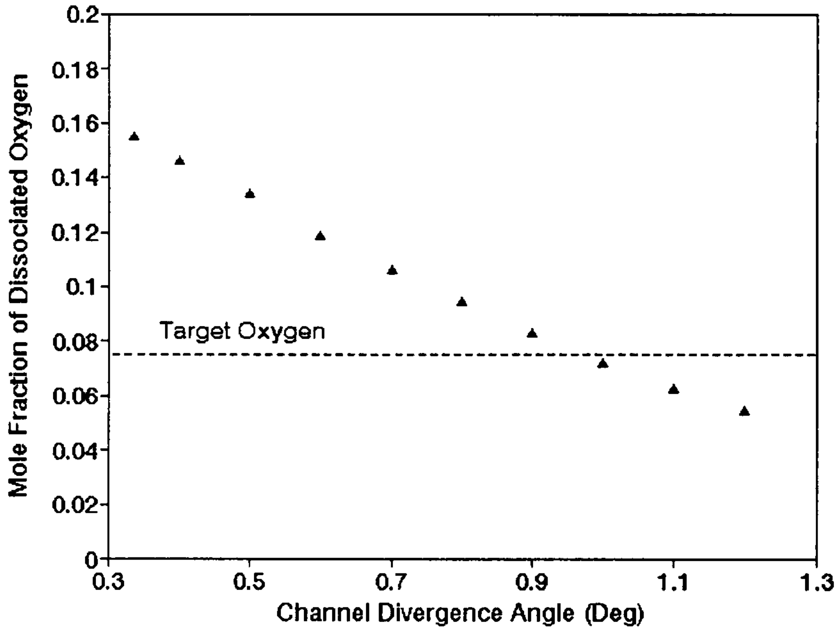

Figure 4.12 : Dissociated Oxygen versus Channel Divergence Angle

0.335° to 0.8° appears to satisfy the target value of 2642 K. Figure 4.12 shows that the mole fraction of dissociated oxygen decreases as the accelerator divergence angle increases. The target value of a 0.075 mole fraction of oxygen is meet between 0.9° and 1.0° of divergence.

The best test case was produced with an accelerator channel divergence angle of 0.8°. The temperature condition is met, the entropy is reduced, and the amount of dissociated oxygen is reduced by 39%. The combustor inlet static temperature, oxygen dissociation, and entropy for this case are:

$$T = 2676 \text{ K}, \quad X_O = 0.0947, \quad \text{and } s = 9.89 \text{ kJ/kg K}$$

Table 4.5 shows the performance results for a divergence angle of 0.8°, and figure 4.13 plots the accelerator performance on the entropy versus total enthalpy map.

Table 4.5 : Accelerator Performance (Angle = 0.8°)

Parameter	Inlet	Exit
Static Pressure (atm)	20.00	1.31
Static Temperature (K)	3255	3329
Velocity (m/sec)	2305	5998
Density (kg/m^3)	2.149	0.132
Ratio of Specific Heats	1.204	1.166
Conductivity (mho/m)	56.45	301.0
Entropy (kJ/kg K)	8.86	9.88
Total Enthalpy (MJ/kg)	6.63	22.73
Total Pressure (atm)	185.8	9627
Mach Number	2.163	5.548
Current Density (amps/cm^2)	22.50	
Specific Heat Flux (kw/cm^2)	3.84	
Total Power (MW)	423	

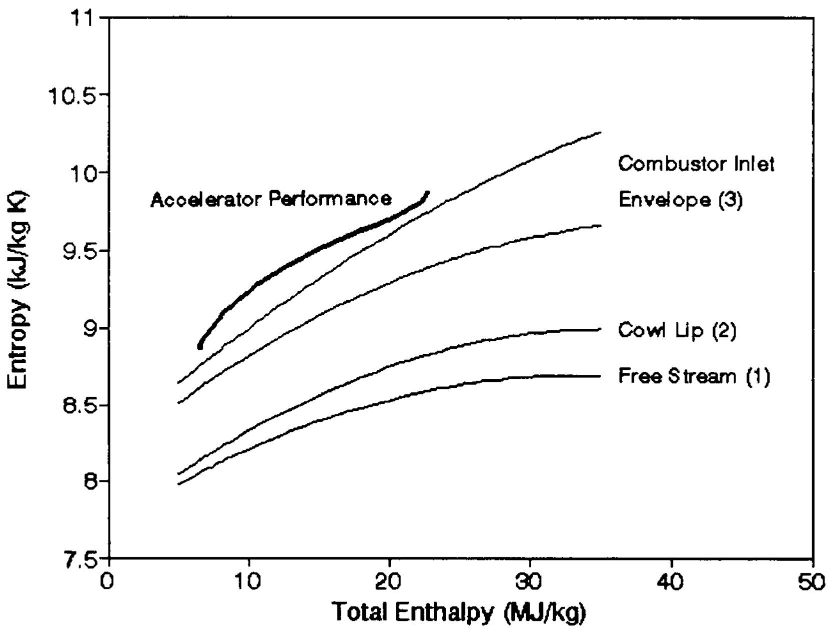

Figure 4.13 : Accelerator Performance (Angle = 0.8°)

4.4 Magnetic Field Strength

The accelerating force in the MHD accelerator is proportional to J x B, and one of the primary loss factors is the Joule heating due to the current flow through the plasma resistance which is proportional to J^2/σ (Crawford, Chapman, and Rhodes, 1990). Therefore, increasing the magnetic field will increase velocity without excessive heating of the driven gas, to produce more efficient acceleration. This in turn reduces the increase of entropy through the channel and produces a lower final entropy and temperature.

The effect of magnetic field strength was examined in the previous UTSI report with magnetic fields ranging from 6 to 10 Tesla. Magnet size was limited by cost (estimated to be proportional to B^2) and then-current state of the art for superconducting magnets. However, new high temperature superconducting materials have high magnetic field cut offs, as high as 80-90 Tesla, when operated at liquid helium temperatures. Using this technology it may be possible to produce magnets with fields of 10-20 Tesla for MHD acceleration. Of course cost is a still considerable issue, but the technology is possible for higher field strength magnets. Therefore, this report again examines magnetic field strength with calculations from 8 to 26 Tesla.

After running the accelerator code with different magnetic field strengths and determining the necessary current densities, figures 4.14 and 4.15 were produced. Figure 4.14 shows the necessary current density for each magnetic field strength.

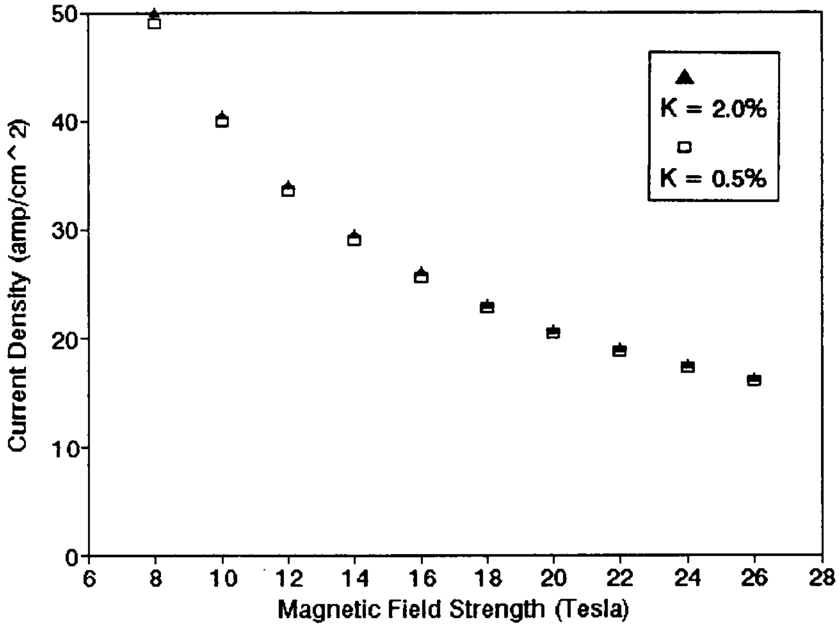

Figure 4.14 : Current Density versus Magnetic Field Strength

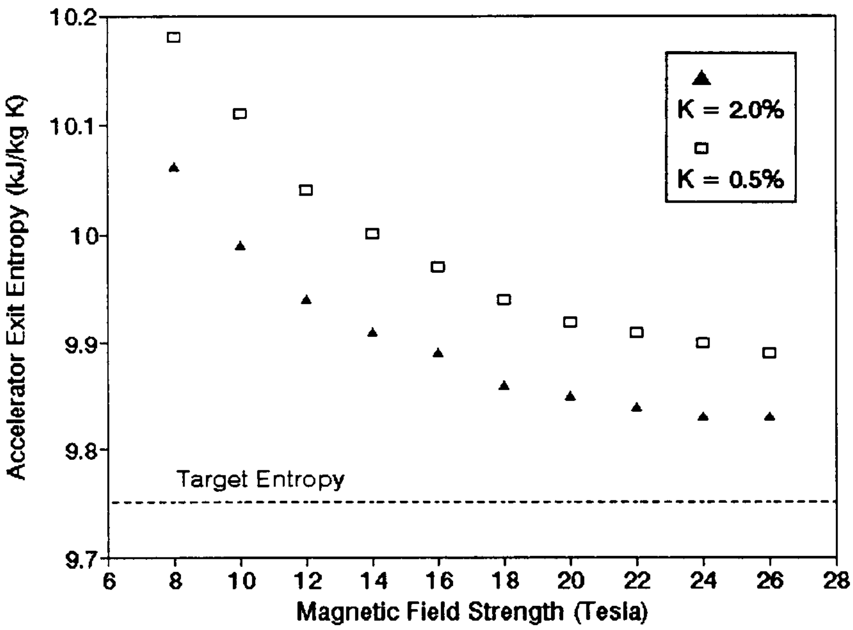

Figure 4.15 : Exit Entropy versus Magnetic Field Strength

As the magnetic field strength increases, the value of current density needed decreases. Figure 4.15 plots the final entropy versus the magnetic field strength. As the magnetic field increases, the benefits gained in entropy reduction lessens. That is, higher fields result in lower entropy but the rate of decrease of entropy with increases in field strength diminishes with increasing field strength. This leads to the conclusion that it is not feasible or economical to keep raising the magnet strength indefinitely in hopes of large entropy reduction. As in the previous test studies, the current density required for 0.5 percent potassium seed is similar to that required by the 2.0 percent seed, and the entropies are approximately 1% higher in the 0.5 percent case.

The flow is then expanded through the downstream nozzle to a static pressure of 0.5 atm to reach the combustor inlet conditions. Figure 4.16 shows that the nozzle area ratio does not change much as the magnetic field strength is increased. The ratio of the exit area to the inlet area ranges between 5.0 and 4.5. The properties of the flow after the expansion are plotted in figures 4.17 and 4.18.

Figure 4.17 shows that the temperature decreases as the magnetic field strength is increased. In fact, the temperature can be reduced far below the target value, unlike in the other two trade-off studies. The temperature value of 2642 K can be satisfied between 8 and 12 Tesla. Figure 4.18 shows that the mole fraction of dissociated oxygen does not decrease very much as the magnetic field strength increases. In fact, it seems to level off at a mole fraction of approximately 0.11.

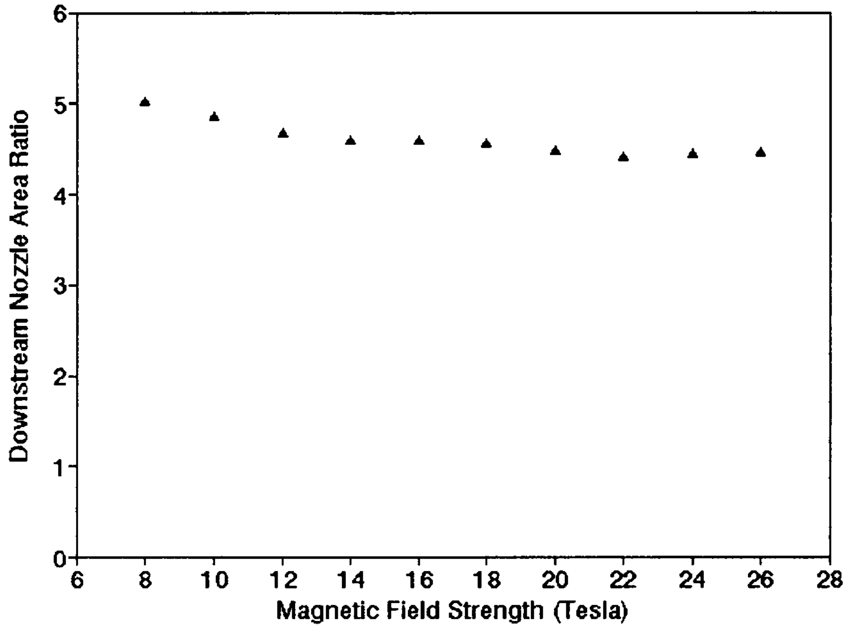

Figure 4.16 : Downstream Nozzle Area Ratio versus Magnetic Field Strength

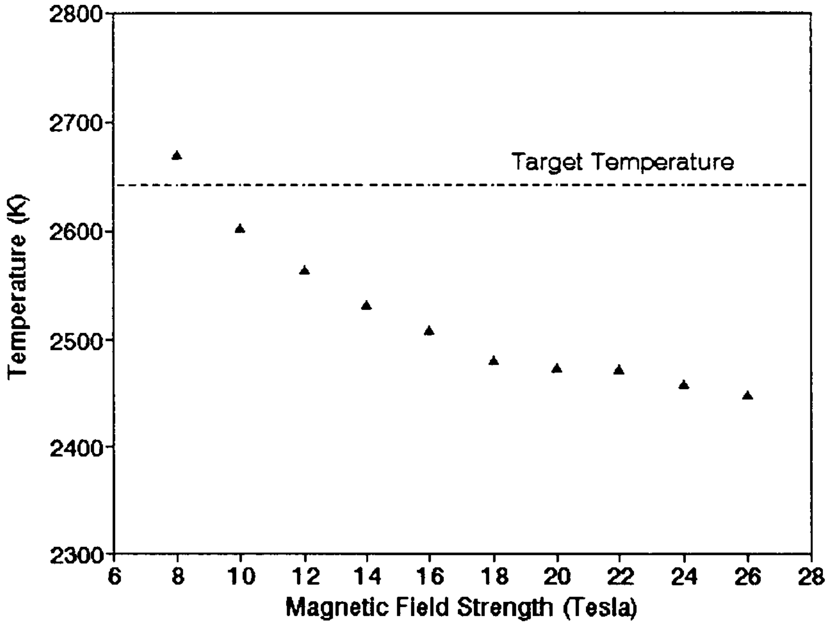

Figure 4.17 : Temperature versus Magnetic Field Strength

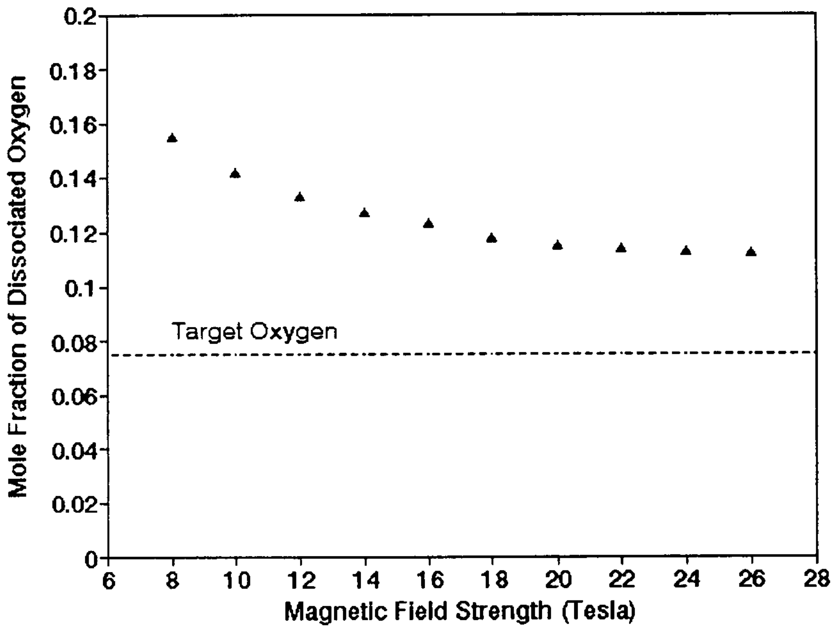

Figure 4.18 : Dissociated Oxygen versus Magnetic Field Strength

The best test case produced by varying the magnetic field strength occurs at 12 Tesla. The temperature condition is satisfied, but the entropy and oxygen dissociation are still high. The resulting combustor inlet values of static temperature, oxygen dissociation, and entropy for this case are:

$$T = 2564 \text{ K}, \quad X_O = 0.1324, \quad \text{and } s = 9.96 \text{ kJ/kg K}$$

The accelerator performance results for the 12 Tesla case are given in Table 4.6. Figure 4.19 shows the performance results on the entropy versus final enthalpy map.

Table 4.6 : Accelerator Performance (12 Tesla Field)

Parameter	Inlet	Exit
Static Pressure (atm)	20.00	3.85
Static Temperature (K)	3255	3850
Velocity (m/sec)	2305	5738
Density (kg/m^3)	2.149	0.325
Ratio of Specific Heats	1.204	1.181
Conductivity (mho/m)	56.45	311.6
Entropy (kJ/kg K)	8.86	9.94
Total Enthalpy (MJ/kg)	6.63	22.59
Total Pressure (atm)	187.5	6226
Mach Number	2.163	4.821
Current Density (amps/cm^2)	34.00	
Specific Heat Flux (kw/cm^2)	7.90	
Total Power (MW)	454	

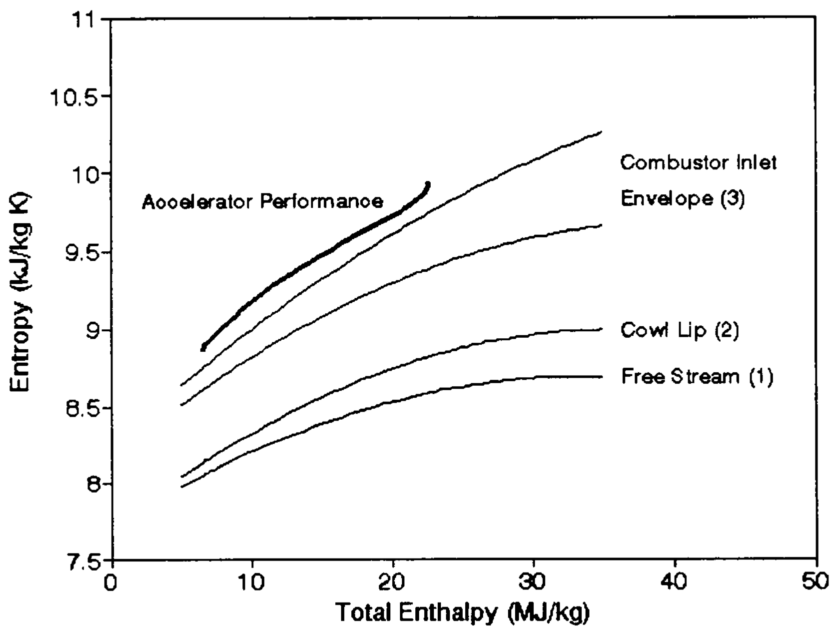

Figure 4.19 : Accelerator Performance (12 Tesla Field)

4.5 Optimum Accelerator Configuration

The trade-off studies presented in this thesis show that the MHD augmented wind tunnel can provide better simulation of the NASP combustor inlet conditions than reported in the previous UTSI study. However, no single case examined was able to meet all three of the investigational goals of the thesis. By manipulating the inlet Mach number and channel divergence angle, the goal of reducing the oxygen dissociation by 50% was met, this is actually a result of lowering the static pressure. Increasing the magnetic field strength greatly reduced the static temperature, but the oxygen dissociation remained high. In no case was the 0.5 percent potassium seed feasible, due to the high entropies it produced.

By using a combination of the studies performed, a configuration which can satisfy all the goals is found. To accomplish this the inlet Mach number or the channel divergence angle cases is increased until the static pressure decreases enough to give the correct oxygen dissociation simulation. The magnetic field strength is then optimized to lower the static temperature and the increase accelerator efficiency. A magnetic field of 16 Tesla was chosen as a feasible limit with current technology. All calculations were performed for both the 2.0% K and 0.5% K seed concentrations.

The first case uses the accelerator inlet Mach 3.38 input values. The results of varying the magnetic field strength with an accelerator inlet Mach number of 3.38 are presented in figures 4.20, 4.21, and 4.22. Figure 4.20 plots the static

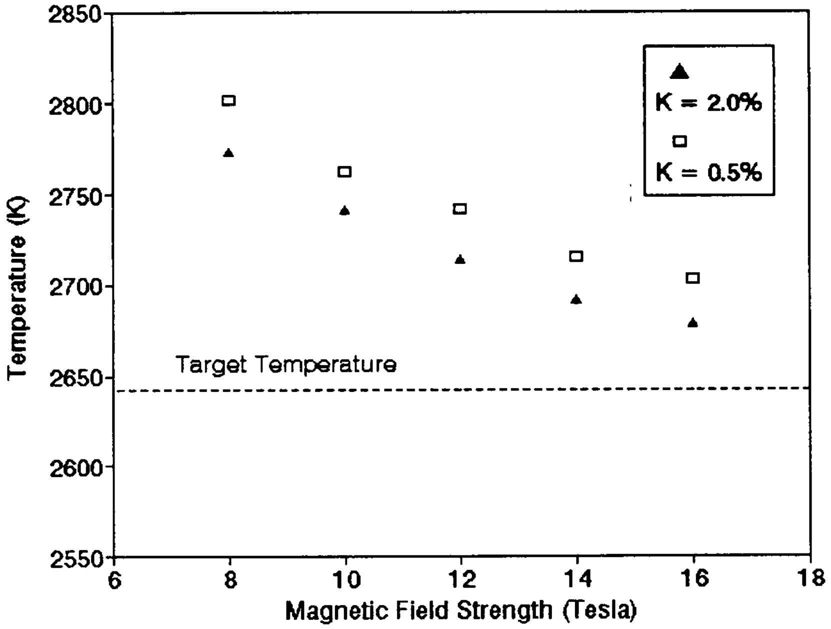

Figure 4.20 : Temperature versus Magnetic Field Strength (Mach = 3.38)

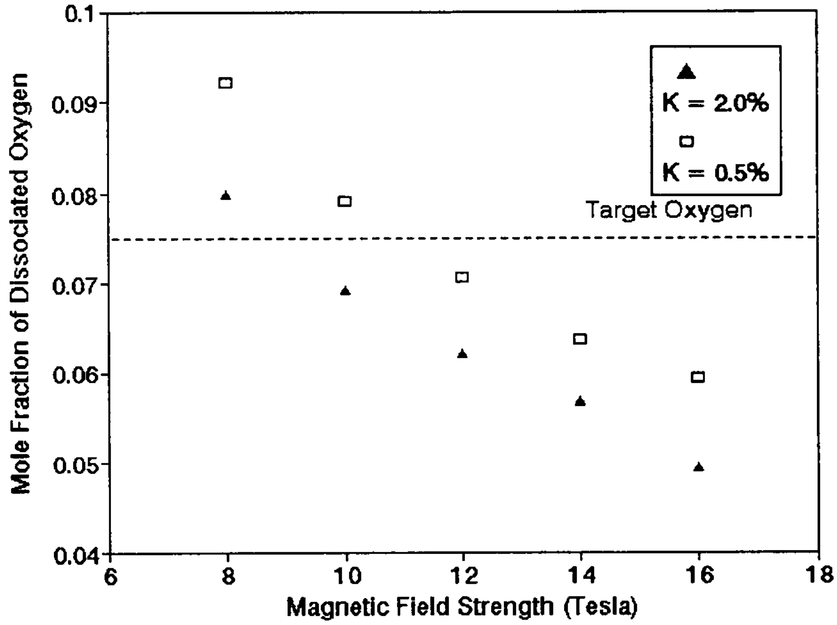

Figure 4.21 : Dissociated Oxygen versus Magnetic Field Strength (Mach = 3.38)

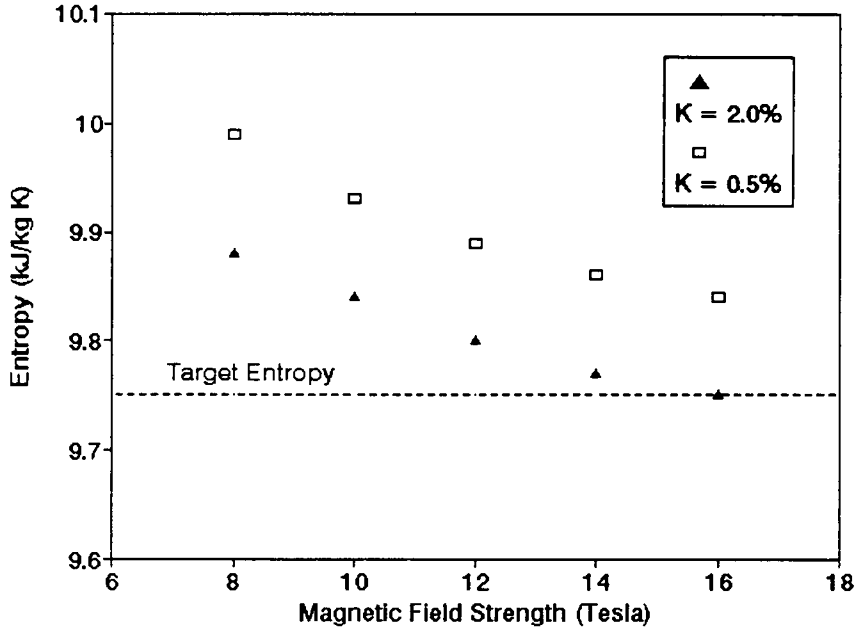

Figure 4.22 : Entropy versus Magnetic Field Strength (Mach = 3.38)

temperature at the combustor inlet versus the magnetic field strength. At 16 Tesla, both the 2.0 and 0.5 percent potassium cases are near the target temperature value, although they are still about 50 degrees too high. Figure 4.21 plots the amount of dissociated oxygen versus the magnetic field strength. The entire range from 10 to 16 Tesla seems to satisfy the dissociated oxygen condition for both the 2.0 and 0.5 percent potassium cases. Figure 4.22 plots the entropy at the combustor inlet versus the magnetic field strength. The 2.0 percent potassium case satisfies the entropy condition at 16 Tesla, while the 0.5 percent case is still about 10% to high at this point.

The best results with an inlet Mach number of 3.38 are obtained with a magnetic field strength of 16 Tesla and a potassium seed concentration of 2.0

percent. The combustor inlet values of static temperature, oxygen dissociation, and entropy for this case are:

$$T = 2678 \text{ K}, \quad X_O = 0.0494, \quad \text{and } s = 9.75 \text{ kJ/kg K}$$

The temperature is approximately 35 degrees above the target value, but the oxygen dissociation and entropy are well simulated. A good simulation could not be produced with the 0.5 percent potassium seed content. Table 4.7 gives the performance results for this case, while figure 4.23 plots the results on the entropy versus total enthalpy map.

The second test case involves varying the magnetic field strength with a channel divergence angle of 0.9°. The results of this study are presented in figures 4.24, 4.25, and 4.26. Figure 4.24 plots the static temperature at the combustor inlet versus the magnetic field strength and shows that the temperature is well simulated over the range of 10 to 16 Tesla for both seed concentration cases, with the best simulation occurring between 12 and 14 Tesla. Figure 4.25 plots the oxygen dissociation versus the magnetic field strength. Again, the range from 10 to 16 Tesla show good simulation of the combustor inlet conditions for both the 2.0 percent and 0.5 percent potassium cases. Figure 4.26 plots the entropy at the combustor inlet versus the magnetic field strength. The 2.0 percent potassium concentration satisfies the entropy condition from 12 to 16 Tesla, while the 0.5 percent potassium concentration satisfies the entropy condition at 16 Tesla.

Table 4.7 : Accelerator Performance (Mach = 3.38, 16 Tesla Field)

Parameter	Inlet		Exit
Static Pressure (atm)	2.00		0.87
Static Temperature (K)	2133		3036
Velocity (m/sec)	2975		6125
Density (kg/m^3)	0.331		0.098
Ratio of Specific Heats	1.267		1.170
Conductivity (mho/m)	2.57		294.7
Entropy (kJ/kg K)	8.87		9.76
Total Enthalpy (MJ/kg)	6.62		22.70
Total Pressure (atm)	162		12939
Mach Number	3.380		5.986
Current Density (amps/cm^2)		5.85	
Specific Heat Flux (kw/cm^2)		2.23	
Total Power (MW)		410	

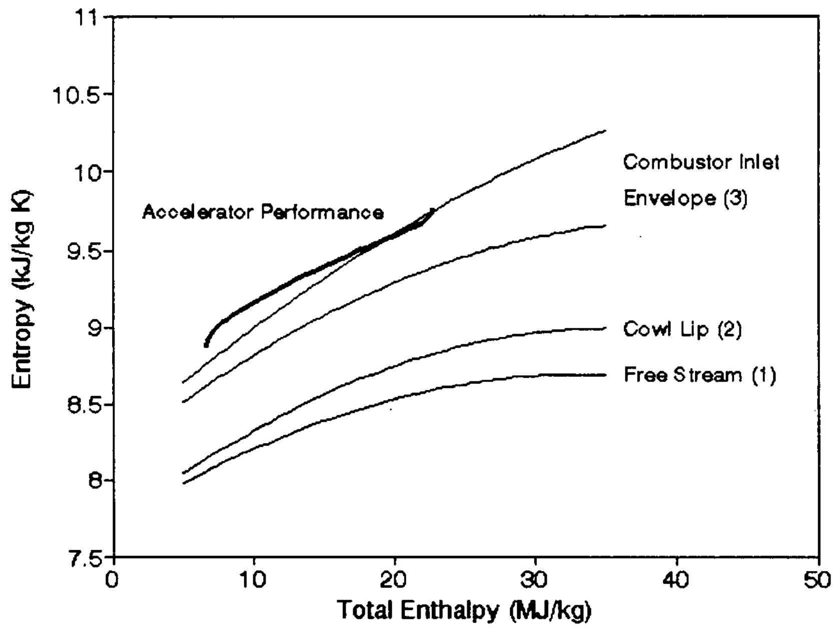

Figure 4.23 : Accelerator Performance (Mach = 3.38, 16 Tesla Field)

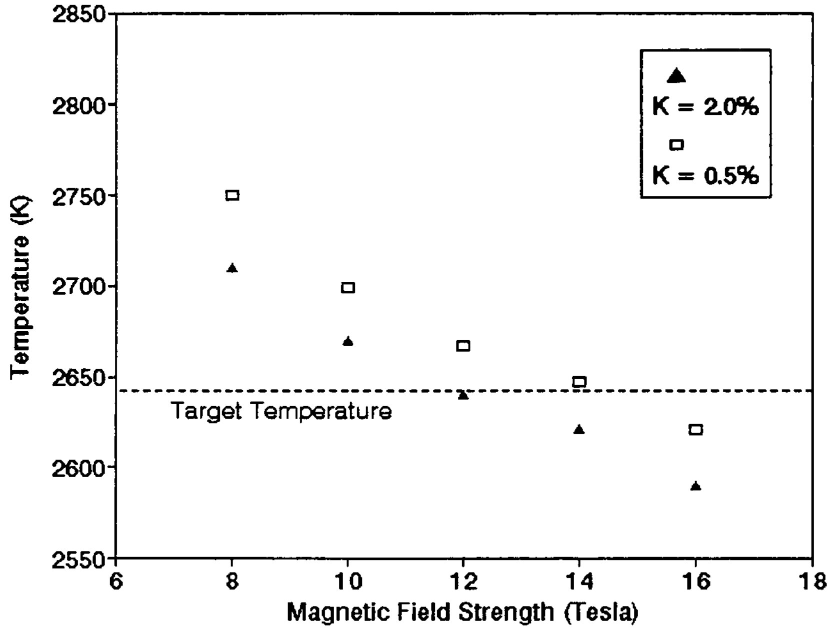

Figure 4.24 : Temperature versus Magnetic Field Strength (Angle = 0.9°)

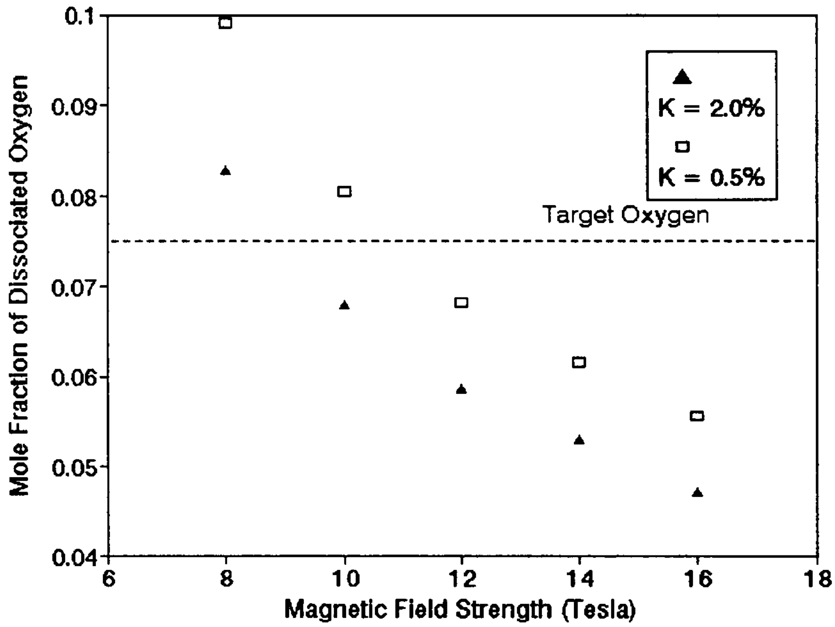

Figure 4.25 : Dissociated Oxygen versus Magnetic Field Strength (Angle = 0.9°)

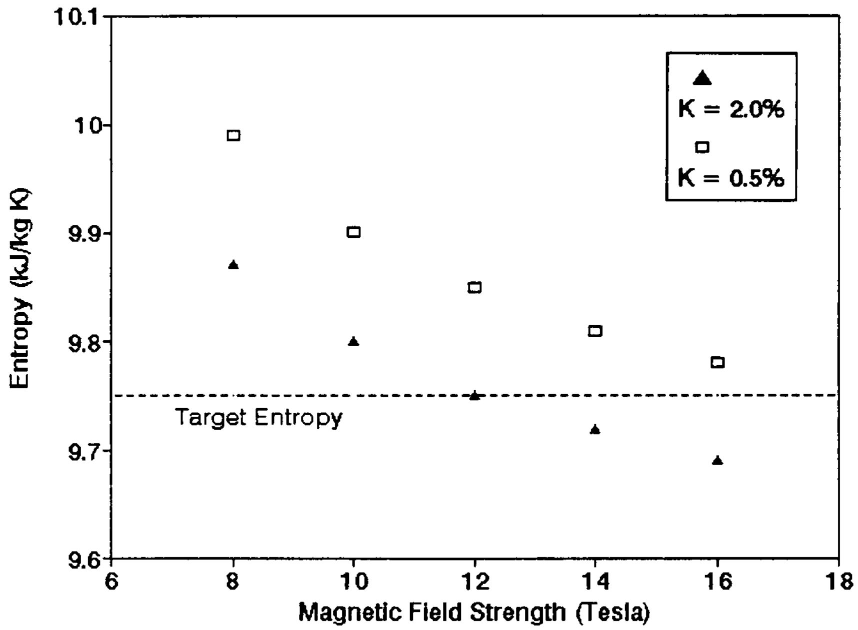

Figure 4.26 :Entropy versus Magnetic Field Strength (Angle = 0.9°)

Two good solutions were produced with the channel divergence of 0.9°, one with 2.0 percent potassium seed, and one with 0.5 percent potassium seed. The best case produced with 2.0 percent potassium is at a magnetic field strength of 12 Tesla. The combustor inlet values of static temperature, oxygen dissociation, and entropy are:

$$T = 2640 \text{ K}, \; X_O = 0.0587, \; \text{and } s = 9.75 \text{ kJ/kg K}$$

This configuration satisfies all of the combustor inlet target conditions, but does not reduce the amount of potassium seed in the flow. Performance results are presented in table 4.8 and plotted on the entropy versus total enthalpy map in figure 4.27.

Table 4.8 : Accelerator Performance (Angle = 0.9°, 12 Tesla Field, 2.0% K)

Parameter	Inlet	Exit
Static Pressure (atm)	20.00	1.02
Static Temperature (K)	3238	3094
Velocity (m/sec)	2291	6089
Density (kg/m^3)	2.162	0.113
Ratio of Specific Heats	1.205	1.170
Conductivity (mho/m)	54.17	295.4
Entropy (kJ/kg K)	8.85	9.75
Total Enthalpy (MJ/kg)	6.56	22.61
Total Pressure (atm)	198	12973
Mach Number	2.156	5.889
Current Density ($amps/cm^2$)	13.25	
Specific Heat Flux (kw/cm^2)	3.30	
Total Power (MW)	416	

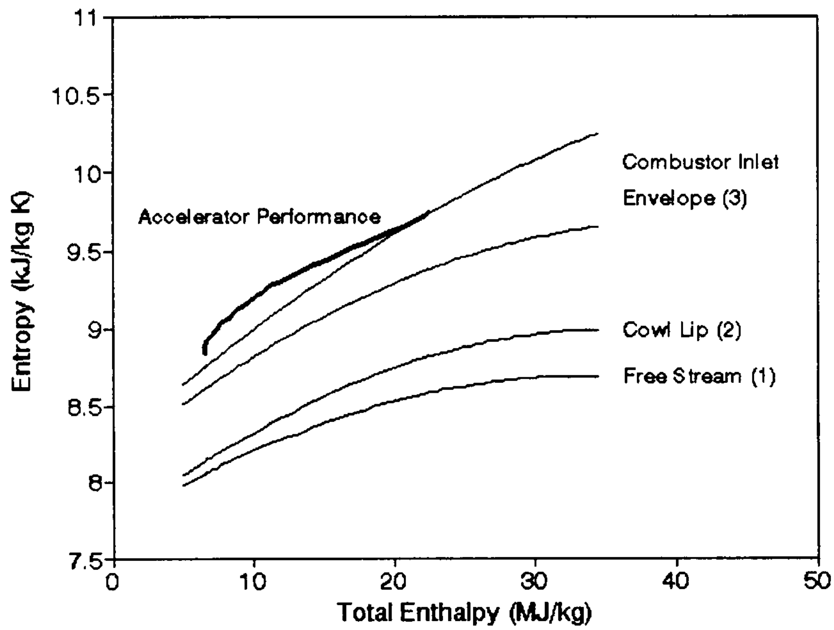

Figure 4.27 : Accelerator Performance (Angle = 0.9°, 12 Tesla Field, 2.0% K)

The second solution found with the 0.9° channel divergence angle meets all the combustor inlet target conditions and reduces the potassium seed to 0.5 percent by weight. This occurs with a magnetic field strength of 16 Tesla. The combustor inlet values of static temperature, oxygen dissociation, and entropy are:

$$T = 2621 \text{ K}, \quad X_O = 0.0557, \quad \text{and } s = 9.78 \text{ kJ/kg K}$$

Again the performance results are presented in table 4.9 and are plotted in figure 4.28 on the entropy versus total enthalpy map. This case seems to be the best configuration presented in this thesis since it meets all of the investigational goals. The amount of potassium seed required is reduced to 0.5 percent by weight, and the temperature and oxygen dissociation are simulated very well.

The configurations that satisfy all the target conditions are not limited to those presented in this section. By manipulating the variables many satisfactory configuration could be attained. For example, a case could be developed which would increase the inlet mach number, divergence angle, and magnetic field strength, which may require a smaller amount of potassium seed to meet the target conditions. What is shown here is only to demonstrate that satisfactory simulation can be obtained.

Table 4.9 : Accelerator Performance (Angle = 0.9°, 16 Tesla Field, 0.5% K)

Parameter	Inlet	Exit
Static Pressure (atm)	20.00	1.01
Static Temperature (K)	3238	3072
Velocity (m/sec)	2302	6120
Density (kg/m^3)	2.151	0.112
Ratio of Specific Heats	1.204	1.170
Conductivity (mho/m)	35.20	296.1
Entropy (kJ/kg K)	8.86	9.78
Total Enthalpy (MJ/kg)	6.59	22.73
Total Pressure (atm)	199.6	13686
Mach Number	2.162	5.931
Current Density ($amps/cm^2$)	10.00	
Specific Heat Flux (kw/cm^2)	3.32	
Total Power (MW)	418	

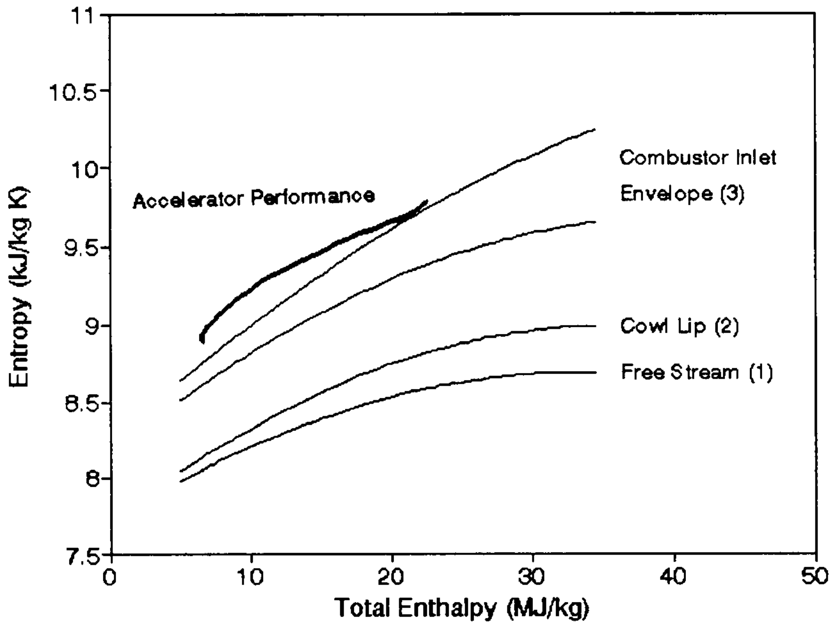

Figure 4.28 : Accelerator Performance (Angle = 0.9°, 16 Tesla Field, 0.5% K)

4.6 Results for Other Mach Numbers

The initial UTSI report on MHD accelerator use for hypersonic testing concluded that a single channel geometry could produce high Mach number simulation capability over a large range (15-25) by varying only the applied electrode power and the downstream nozzle area (Crawford, Chapman, and Rhodes, 1990). While this is generally true, it was found that the simulation conditions at Mach 25 and Mach 15 were not nearly as good as those for the Mach 20 baseline case. This is an important result to prove, as it makes the cost-benefits of the MHD accelerator facility more attractive. In this section the problem of correctly simulating the Mach 25 and Mach 15 case are examined.

To simulate the Mach 25 combustor inlet conditions, the flow must leave the accelerator channel with a total enthalpy of 34.5 MJ/kg. After expansion through the downstream nozzle, a static pressure of 0.47 atm and a static temperature of 3300 K are needed to meet the combustor inlet target conditions that were calculated by the John Hopkins University Applied Physics Laboratory (1986). All three of the optimized accelerator designs from Section 4.5 produced very poor simulation results, with temperatures about 500 K too low for the Mach 25 case.

It was found that much better simulations could be reached by lowering the magnetic field strength, which in turn increased the static temperature, while having a minimal effect on the oxygen dissociation. The combustor inlet conditions that best simulated the target values were produced in a channel with the following characteristics:

Inlet Mach = 2.160, Divergence Angle = 0.9°, Field = 4 Tesla, K = 2.0%

After expansion through the downstream nozzle to a static pressure of 0.47 atm, the following combustor inlet values of static temperature, oxygen dissociation, and entropy were produced:

$$T = 3178 \text{ K}, \quad s = 10.59 \text{ kJ/kg K}, \quad X_o = 0.2426$$

The accelerator performance is presented in table 4.10 and is plotted on the entropy versus total enthaply map in figure 4.29.

The Mach 15 case proves to be much more difficult with the current accelerator configuration. To simulate this condition the flow must leave the accelerator with a total enthalpy of 11.50 MJ/kg. The expansion to the combustor inlet, should produce a static pressure of 0.56 atm and a static temperature of 1909 K according to the John Hopkins University Applied Physics Laboratory (1986). After performing the trade-off studies presented in this chapter for the Mach 15 case, it was found that the static temperature was too high in all cases.

The best test configuration occurred with an accelerator channel with the following characteristics:

Inlet Mach = 2.74, Divergence Angle = 0.335°, Field = 16 Tesla, K = 2.0%

Table 4.10 : Accelerator Performance (Mach 25 Simulation)

Parameter	Inlet	Exit
Static Pressure (atm)	20.00	1.04
Static Temperature (K)	3255	3662
Velocity (m/sec)	2305	7530
Density (kg/m^3)	2.149	0.091
Ratio of Specific Heats	1.204	1.174
Conductivity (mho/m)	56.45	316.6
Entropy (kJ/kg K)	8.86	10.36
Total Enthalpy (MJ/kg)	6.61	34.50
Total Pressure (atm)	200.0	32395
Mach Number	2.163	6.455
Current Density (amps/cm^2)	36.50	
Specific Heat Flux (kw/cm^2)	4.47	
Total Power (MW)	698	

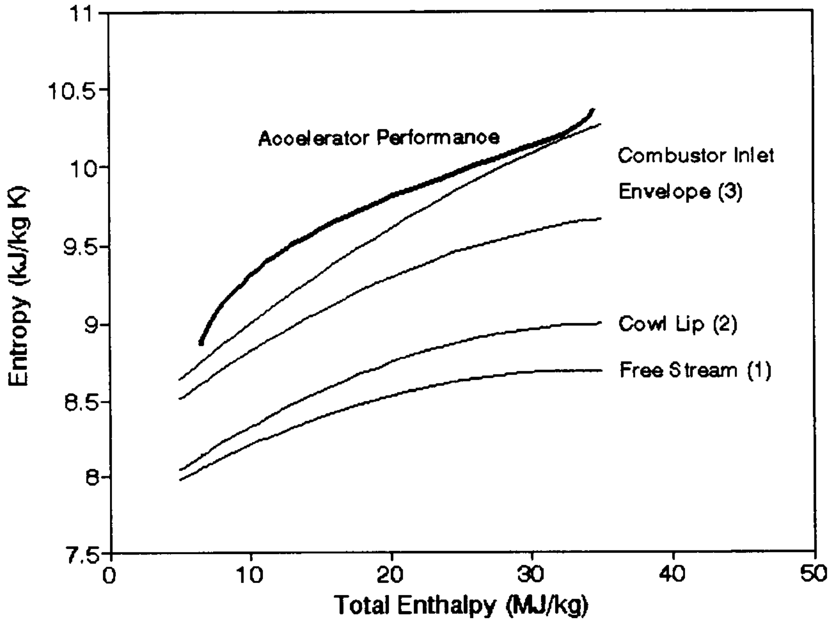

Figure 4.29 : Accelerator Performance (Mach 25 Simulation)

After expansion through the downstream nozzle to a static pressure of 0.56 atms, the following combustor inlet values of static temperature, oxygen dissociation, and entropy were produced:

$$T = 2119 \text{ K}, \quad s = 9.33 \text{ kJ/kg K}, \quad X_O = 0.0248$$

Even in this case the static temperature is about 200 K higher than needed for the correct simulation. The performance results for this accelerator channel are presented in table 4.11, and are plotted on the entropy versus total enthalpy map in figure 4.30.

Table 4.11 : Accelerator Performance (Mach 15 Simulation)

Parameter	Inlet	Exit
Static Pressure (atm)	6.67	2.45
Static Temperature (K)	2703	2963
Velocity (m/sec)	2678	3941
Density (kg/m^3)	0.870	0.289
Ratio of Specific Heats	1.229	1.192
Conductivity (mho/m)	20.60	290.4
Entropy (kJ/kg K)	8.86	9.33
Total Enthalpy (MJ/kg)	6.61	11.34
Total Pressure (atm)	186.9	642.8
Mach Number	2.742	3.891
Current Density (amps/cm^2)	6.25	
Specific Heat Flux (kw/cm^2)	2.92	
Total Power (MW)	154	

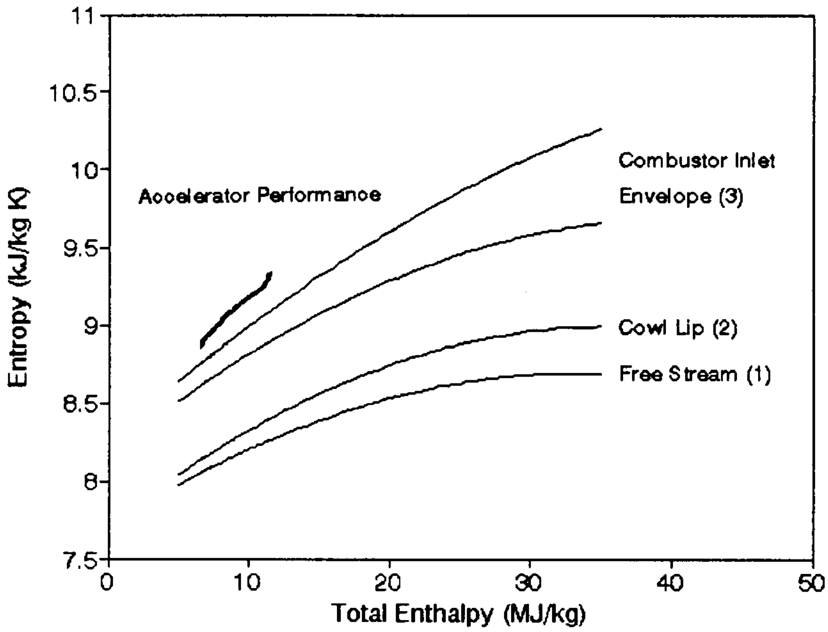

Figure 4.30 : Accelerator Performance (Mach 15 Simulation)

5.0 CONCLUSIONS AND RECOMMENDATIONS

5.1 Channel Design Trade-Off Study Conclusions

Throughout this thesis a number of conclusions were discovered about the general behavior of the MHD accelerator simulation facility when the channel inlet Mach number, channel divergence area, and magnetic field strength are varied. In addition, a better understanding was gained of the range in which the MHD accelerator facility provides the best simulation conditions. Following is a list of the conclusions made from this thesis.

- Reducing the static pressure in the accelerator channel, either by increasing the accelerator channel inlet Mach number or increasing the channel divergence angle, significantly reduces the amount of dissociated oxygen in the flow.

- Increasing the magnetic field strength reduces the static temperature of the flow, but the effect diminishes at higher magnetic fields.

- The flow entropy can be reduced by increasing the accelerator channel inlet Mach number, increasing the accelerator channel divergence angle, or increasing the magnetic field strength.

- The amount of potassium seed needed can be reduced to at least 0.5 percent by mass with careful design of the accelerator channel under the assumption that diffuse current transport can be maintained at low conductivity levels.

- Flows can be produced that accurately simulate the conditions at the combustor inlet of a NASP propulsion test module.

The goals of this thesis were to study conditions for a MHD accelerator which would (1) reduce the amount of seed used in the flow, (2) reduce the temperature in the test section, and (3) reduce the oxygen dissociation in the test section. Examination of these conclusions shows that the investigational goals of this thesis have been met. However, another area of concern was noticed. The low conductivity levels that accompany reduced static pressure may seriously impact accelerator performance by an inability to maintain diffuse current transport rather than constricted arc transport. The low conductivity levels also increase power requirements for the accelerator and in general exhibit high Joule heating losses in the accelerator inlet regions. This heating in turn increases the conductivity with an accompanying increase in the entropy.

5.2 Recommendations for Future Study

This thesis has further proven the capabilities and technical feasibility of the MHD augmented hypersonic simulation facility. However, further research is needed before a full scale prototype can be attempted. The following is a list of recommendations for the future study of this problem.

- Continue to examine the configuration of the accelerator channel. By manipulating other variables of the channel and flow, more can be learned about reaching the correct simulation conditions.

- Develop an accelerator configuration which better simulates the combustor inlet conditions for the Mach 15 and Mach 25 cases. The ability to test over a wide range of Mach numbers will be critical to the economic feasibility of the facility.

- A three-dimensional accelerator code is needed in order to understand the three-dimensional coupled fluid mechanics and electromagnetic effects.

- Sub-scale laboratory experiments are required to improve understanding of some of the technical issues involved. These issues include current density limits, minimum conductivity limits, viscous losses, and wall heat transfer. This information can be used to improve the existing and future accelerator models.

- Finally, an experimental MHD accelerator facility must be developed to address critical technology issues needed to better understand how to design a full-scale facility.

LIST OF REFERENCES

Alfyor, V. "A Report of the Status of MHD Hypersonic Ground Test Technology in Russia." AIAA 93-3193, July, 1993.

Billig, F.S., et al. "Proposed Supplement to Propulsion System Management Support Plan." Johns Hopkins University Applied Physics Laboratory, Laurel, Maryland, 1986.

Crawford, R.A., Chapman, J.N., and Rhodes, R.P. "Potential Application of Magnetohydrodynamic Acceleration to Hypersonic Environmental Testing." Calspan Subcontract No. 89-04, 1990.

Gordon, S. and McBribe, B.J. "Computer Program for Calculation of Complex Chemical Equilibrium Compositions, Rocket Performance, Incident and Reflected Shocks, and Chapman-Jouguet Detonation." NASA SP-273, 1971.

Lineberry, J., and Chapman, J. "MHD Accelerators for Hypersonic Applications." AIAA 91-0384, January, 1991.

Mikatarian, R.R., Kau, C.J., and Pergament, H.S. "A Fast Computer Program for Nonequilibrium Rocket Plume Predictions." AeroChem TP-282, August 1972.

Richey, K. and McKinney, L.W. "Hypersonic Test Investment Plan (HTIP)" Micro Craft, Inc., Tullahoma, Tennessee, May 1993

Ring, L.E. "General Considerations of MHD Acceleration for Aerodynamic Testing." AEDC-TR-64-256 (AD453419), December 1964.Rosa, R.J. Magnetohydrodynamic Energy Conversion. McGraw-Hill Book Company, New York, 1968.

Shercliff, J.A. A Textbook of Magnetohydrodynamics. Pergamon Press, London, England, 1965

Waltrup, P.J., Billig, F.S., and Stockbridge, R.D. "Engine Sizing and Integration Requirements for Hypersonic Airbreathing Missile Applications." AGARD Propulsion and Energetics Panel, 58th Symposium, Ramjet and Ramrockets for Military Applications, London, England, October 26-30, 1987.

VITA

Michael John Christiansen was born on March 17, 1971 in Fond du Lac, Wisconsin. He is the first of two children raised by his parents John and Marilyn. He graduated with High Honors from L.P. Goodrich High School in Fond du Lac, Wisconsin in June, 1989. Michael then enrolled in the Mechanical Engineering Program at the Milwaukee School of Engineering (MSOE), Milwaukee, Wisconsin. While at MSOE, Michael completed his Senior Design Project entitled, "Maximization of Payload Lifted by a Radio Controlled Airplane" complete with a working prototype with partners Andy Broeren, John Schultz, and David Stone. He graduated from MSOE with high honors in May, 1993, second in the Mechanical Engineering Class.

Following his undergraduate work, Michael accepted a Graduate Engineering Assistanceship from the University of Tennessee Space Institute (UTSI). He enrolled in the Mechanical Engineering Masters Program. While at UTSI Michael become highly involved in the Student Government Association, holding both the Vice-Presidential and Presidential positions. Michael completed his thesis and graduated from UTSI in August, 1995.